東京大学大学院新領域創成科学研究科

環境学研究系自然環境学専攻

地球海洋環境学分野

2009 年度

修士論文

Development and application of paleoenvironmental proxy in biogenic calcium carbonate

（生物源炭酸塩の古環境間接指標の開発と応用）

2009 年 7 月 7 日提出

2009 年 9 月修了

指導教員　川幡穂高 教授

076887　吉村寿紘

Contents

Part Ⅰ

“Oxygen and carbon isotope records of cultured freshwater pearl mussel *Hyriopsis* sp. shell from Lake Kasumigaura, Japan”

（霞ヶ浦産淡水真珠貝 *Hyriopsis* sp.の酸素・炭素同位体比）

published: Yoshimura, T., Nakashima, R., Suzuki, A., Tomioka, N. and Kawahata, H. (2009) Oxygen and carbon isotope records of cultured freshwater pearl mussel Hyriopsis sp. shell from Lake Kasumigaura, Japan. Journal of Paleolimnology, DOI 10.1007/s10933-009-9341-8.

Part Ⅱ

“Mg isotope composition of hermatypic and deep-sea corals”

（造礁・深海サンゴの Mg 同位体組成）

List of Figures and Tables

Part Ⅰ

Part Ⅱ

Part Ⅰ: Oxygen and carbon isotope records of cultured freshwater pearl mussel *Hyriopsis* sp. shell from Lake Kasumigaura, Japan

1 Introduction

In Lake Kasumigaura (36°04'N, 140°40'E), the freshwater pearl mussel *Hyriopsis* sp. (Bivalvia Unionidae) is cultured commercially (Fig. 1). Bivalve pearls as well as their shells are called "biominerals," and they are composed of calcium carbonate. The biominerals of marine and freshwater organisms have been used for paleoenvironmental reconstruction, such as paleo-water temperature and paleosalinity, under the assumption that stable isotope ratios of the biominerals are controlled by physiochemical conditions in the ambient water (Urey 1947; Epstein et al. 1953). Mollusk shells are known to precipitate under close to equilibrium conditions with respect to oxygen isotope ratios (Grossman and Ku 1986). The oxygen isotope ratios of shells depend on both temperature and the oxygen isotope ratios of the ambient water, and marine bivalve shells have been utilized for paleoenvironmental reconstruction (Weidman et al. 1994; Dettman et al. 2004). Shells of freshwater bivalves have also been used as archives of water temperature and isotope hydrology (Dettman et al. 1999; Kaandorp et al. 2003; Goewert et al. 2007). In addition, oxygen isotope ratios of pearls are expected to record their precipitation history, in particular, their growth period and optimal growth temperature (Kawahata et al. 2006). Carbon isotope ratios of shells are controlled mainly by the stable carbon isotope composition of dissolved inorganic carbon (DIC) in the ambient water and the metabolic activity of the bivalves, although the contribution ratio of dissolved inorganic carbon and metabolic carbon is variable (Tanaka et al. 1986; Gillikin et al. 2007). However, environmental information is sometimes incomplete because shell growth of bivalves is not continuous year-round. Owing to discontinuities in accretional growth, it is essential to combine a growth-line analysis with the stable isotope profiles (Jones et al. 1978; Kennish 1980; Jones 1981; Tanabe 1988). Growth lines often form when the growth rate decreases or stops in response to environmental or physiological factors (Kennish 1980). A relationship between growth lines and the oxygen isotopic profile has been documented in some bivalves (Dettman et al. 1999; Schöne et al. 2004; Nakashima et al. 2004). In this study, we describe the shell structure and isotopic records of a cultured freshwater pearl mussel specimen and of a pearl from the specimen. Our aims were (1) to assess the suitability of the shells as an environmental archive, (2) to reconstruct the growth history of the shell, and (3) to determine the growth period of a freshwater pearl. This is the first study presenting the isotopic profile of a freshwater pearl.

2 Materials and Methods

For this study, a live specimen of cultured *Hyriopsis* sp. was collected. To stimulate pearl

production, mantle pieces are inserted into the connective tissue of the mantle. Our specimen had an operation on 7 July 2004, and the pearls were picked out of our specimen on collected date of 25 October 2007. Its shell length and height were 18.5 and 14.9 cm, respectively. Each valve had nine pearls, for a total of 18 pearls. Ordinarily, insert surgery is performed on three-year-old mussels. Therefore, we assumed that our specimen had lived for seven years. We prepared thin sections to investigate the shell structure. The shell mineralogy was ascertained by X-ray diffraction analysis (XRD) with a Flescan diffractometer (RINT2500, Rigaku Co. Tokyo, Japan). We sampled the shell using a dental drill with a 0.4-mm drill bit along the maximum growth axis (177 mm) from umbo to ventral margin at 1-mm intervals. We could not sample the part around the umbo (0–43 mm from the umbo along the maximum growth axis; Fig. 1) because the umbonal surface was eroded. We performed the sampling under microscopic observation to prevent contamination of the samples by the nacreous layer. After microsampling, oxygen and carbon isotope ratios ($\delta^{18}O$ and $\delta^{13}C$) of shell and pearl were measured with an isotope ratio mass spectrometer (Micromass ISOPRIME) equipped with a carbonate device (Micromass Multiprep) at AIST. Isotopic data are reported as per mil (‰) deviations relative to Vienna Peedee belemnite (VPDB). The $\delta^{18}O$ of water ($\delta^{18}O_{WATER}$) was determined for samples collected at three locations near site 1 in the lower Shintone River between June 2005 and December 2006 (Fig. 2). The oxygen isotope ratio of the water was determined by the CO_2–H_2O equilibration technique (Epstein and Mayeda 1953) with an isotope ratio mass spectrometer (Finnigan MAT 252, Thermo Fisher Scientific Inc.) at National Institute for Environmental Studies (NIES). Isotopic data are given in per mil relative to Vienna Standard Mean Ocean Water (V-SMOW). The Deep-sea water (DyDo DRINCO, Inc.) and Ryu-sen-do cave water (Iwaizumi Sangyou Kaihatsu Co., Ltd.) were used as secondary standards for oxygen isotope measurements of lake water samples. The water temperatures were reconstructed from $\delta^{18}O$ values of the outer shell layer and the ambient water using the formula (equation 1) of Grossman and Ku (1986) as modified by Goodwin et al. (2001):

$$T\ (°C) = 20.6 - 4.34(\delta^{18}O_{aragonite} - (\delta^{18}O_{water} - 0.2)), \quad (1)$$

where $\delta^{18}O_{WATER}$ and $\delta^{18}O_{aragonite}$ are expressed relative to VSMOW and VPDB, respectively.

3 Results and Discussion

The $\delta^{18}O$ of water samples ($\delta^{18}O_{WATER}$), sampled from three sites along the Shintone River between June 2005 and December 2006, varied between –8.5‰ and –4.6‰ (Fig. 2). Mean $\delta^{18}O_{WATER}$ values at the three sites along the Shintone River during the observation period were –6.74‰ (site 13), –6.52‰ (site 14), and –6.74‰ (site 15), with an overall average value of –6.49‰. The $\delta^{18}O$ profile of the outer shell layer ($\delta^{18}O_{SHELL}$) varied from –9.6‰ to –3.7‰ and exhibited six first-order cycles (Fig. 1). The first-order fluctuations of $\delta^{18}O_{SHELL}$ were apparently caused by

seasonal changes in water properties. The maximum $\delta^{18}O_{SHELL}$ was around –4‰ in every cycle, which we calculated to reflect a water temperature of 10.7 °C. This result is concordant with the cessation temperature threshold of Wada (1999). The calculated maxmia of water temperature ranged from 26.0 to 33.9 °C. The calculated annual fluctuation range of water temperature based on $\delta^{18}O_{SHELL}$ was 15.3–23.2 °C, which is a quite small range compared with the actual measurement range of 30 °C at site 3 (Fig. 3).

In 2006, measured $\delta^{18}O_{SHELL}$ is correlated well with calculated $\delta^{18}O_{SHELL}$. On the other hand, the measured data showed clear fluctuation exceeding the range of calculated data in 2005. A comparison between measured and calculated $\delta^{18}O_{SHELL}$ indicate that the drastic changes of the $\delta^{18}O_{WATER}$ values occurred with time interval of shorter than at least 2 weeks. There were an inadequate number of shell-carbonate data for 2007 due to the decrease of shell growth ratio. Taking into the fact that the bi-weekly temporal increase or decrease of water temperature due to seasonal change is approximately 2.5°C that corresponds to the $\delta^{18}O$ values of 0.6‰, the bi-weekly maximum fluctuation range of the $\delta^{18}O_{WATER}$ is approximately 2‰ from shell records. The $\delta^{18}O_{WATER}$ of Shin-tone river showed drastic changes of the maximum values of ~2‰ with time spans of shorter than two weeks during summer from 2002 to 2006. If the water temperature was constant during the winter growth cessation period, then the uniform high values of $\delta^{18}O_{WATER}$ suggest a relatively steady precipitation–evaporation balance during the winter dry season across the years. On the other hand, $\delta^{18}O_{SHELL}$ recorded drastic changes in isotopic signatures of ambient water during warm months. The $\delta^{18}O_{SHELL}$ data indicated that the $\delta^{18}O_{WATER}$ of Shin-tone river showed drastic changes of the maximum values of ~2‰ with time spans of shorter than two weeks during summer from 2002 to 2006. And the minima of $\delta^{18}O_{SHELL}$ of 2002 and 2004 are approximately 3‰ lower than those of 2003, 2005, and 2006. Those differences might be caused by the annual difference of isotopic composition of meteoric water during summer. *Hyriopsis* sp. shells can thus potentially be used for paleohydrologic reconstruction.

Moreover, we observed that thick, complete disturbance rings coincided with maxima and minima of the oxygen isotope profile (Fig. 4). Disturbance rings recognized by external observation were associated with several winter and summer, whereas we found no ring on the shell surface corresponding to summer of 2005, however. It is widely known that disturbance rings are formed when growth decreases or stops because of extreme environmental stress or physiological factors (Kennish 1980; Jones and Quitmyer 1996). The co-occurrence of disturbance rings and the winter oxygen isotope profile maxima suggests that this specimen of *Hyriopsis* sp. halted its growth during winter extremes. These findings suggest that summer growth cessation was not caused by seasonal events such as the extremely high summer water temperatures, but by occasional events such as turbid water due to suspension of terrigenous particulate matter accompanying heavy rainfall, as the decrease of dissolved oxygen concentration.

The examined pearl was composed of three couplets, each consisting of a bright and a dark band. The $\delta^{18}O_{PEARL}$ ranged from –7.2‰ to –5.1‰. The $\delta^{18}O$ values of the dark bands were relatively higher than those of the bright bands. We converted the $\delta^{18}O$ values into water temperatures using equation (1), and the calculated temperatures ranged between 13.6 and 22.8 °C. Precipitation temperatures of pearls have been reported only for the most commonly cultured marine pearl oyster *Pinctada fucata martensii* (Kawahata et al., 2006). Marine pearls are produced mainly at around 25 °C. The optimal temperature for freshwater pearl calcification is obviously lower than that for marine pearls. Moreover, precipitation of freshwater pearls may occur over a wider temperature range than precipitation of marine pearls. This may explain the high precipitation rate of freshwater pearls in ambient water with extremely low carbonate saturation levels relative to the waters in which marine pearls are produced.

The $\delta^{13}C$ profile of the outer shell layer ($\delta^{13}C_{SHELL}$) varied from –12.5‰ to –9.2‰ and did not exhibit cyclic fluctuation (Fig. 1). The $\delta^{13}C_{SHELL}$ values varied with an amplitude of >1‰ over the period corresponding to the initial first-order cycle of the $\delta^{18}O_{SHELL}$ profile. In other parts of the shell, amplitudes of $\delta^{13}C_{SHELL}$ variations were <1‰. We observed no secular trend with aging and overall correlation between $\delta^{13}C_{SHELL}$ and $\delta^{18}O_{SHELL}$. The $\delta^{13}C$ values were generally about –10.5‰. Neither a clear annual periodicity nor an ontogenic trend was observed in the $\delta^{13}C$ profile (Fig. 1). The lack of a consistent pattern suggests that body size had only a minor effect on $\delta^{13}C_{SHELL}$ in this species. We can not discuss a metabolic carbon contribution to the shell and whether the isotopic fluctuation of the $\delta^{13}C_{SHELL}$ is driven by isotopic equilibrium or non-equilibrium because of a lack of the $\delta^{13}C$ data of DIC in the ambient water.

4 Conclusion

The number of first-order fluctuations of $\delta^{18}O$ was consistent with the records of the duration of culture. The dominant factor controlling annual $\delta^{18}O$ fluctuations was water temperature with a minor contribution from the variation in the $\delta^{18}O$ of ambient water, especially in the rainy season. The $\delta^{13}C$ values were fairly constant throughout the life of the mussel. A lack of any annual secular trend indicated that the contributions of body size to shell $\delta^{13}C$ values were minor. The presence of distinct disturbance rings coinciding with winter peaks of the oxygen isotope profile indicated that growth ceased at temperatures below approximately 10 °C in winter, probably as a result of the low water temperature or because of reproduction. In contrast, summer disturbance rings suggested that summer growth cessation was caused by occasional events, such as heavy rain, as the decrease of dissolved oxygen concentration. The $\delta^{18}O$ profile and shell structures indicated that the shell aragonite was precipitated at close to oxygen isotope equilibrium with the ambient water. *Hyriopsis* sp. shells can thus potentially be used for hydrologic and shell growth reconstruction. The $\delta^{18}O$

values of the pearl indicated that calcification occurred over a temperature range of at least 13–23 °C. The optimal temperature for freshwater pearl calcification is lower that for marine pearls.

5 Acknowledgments

The author is most grateful to my supervisor, professor Hodaka Kawahata for overall support. I express my first appreciation to Dr. Rei Nakashima of AIST for many helpful advises, valuable discussions and many supports, to Dr. Atsushi Suzuki of AIST for providing the thoughtful comments and advises, and to Dr. Noriko Tomioka of NIST for providing the data of oxygen isotope ratios of lake waters and valuable advises. Special thanks to Mr. Shoichi Kitao of Meiko Pearl Ushiku Co., Ltd. for providing the specimen. We also thank Dr. Kazuo Matsushige of NIES for providing the water temperature data and valuable comments. Special thanks to Natsumi Hokanishi of AIST for performing the measurements of the stable isotopes and to Dr. Mayuri Inoue and Dr. Azumi Kuroyanagi for providing valuable comments and advice.

6 References

Dettman DL, Reische AK, Lohmann,KC (1999) Controls on the stable isotope composition of seasonal growth bands in aragonitic fresh-water bivalves (Unionidae). Geochim Cosmochim Acta 63: 1049-1057

Dettman DL, Flessa KW, Roopnarine PD, Schöne BR, Goodwin DH (2004) The use of oxygen isotope variation in shells of estuarine mollusks as a quantitative record of seasonal and annual Colorado River discharge. Geochim Cosmochim Acta 68: 1253–1263

Epstein SR, Buchsbaum R, Lowentein HA, Urey HC (1953) Revised carbonate-water isotopic temperature scale. Geol Soc Am Bull 64: 1315-1326

Gillikin DP, Lorrain A, Meng L, Dehairs F (2007) A large metabolic carbon contribution to the $\delta^{13}C$ record in marine aragonitic bivalve shell. Geochim Cosmochim Acta 71: 2936-2946

Goewert A, Surge D, Carpenter SJ, Downing J (2007) Oxygen and carbon isotope ratios of *Lampsilis cardium* (Unionidae) from two streams in agricultural watersheds of Iowa, USA. Palaeogeogr Palaeoclimatol Palaeoecol 252: 637-648

Goodwin DH, Flessa KW, Schöne BR, Dettman DL (2001) Cross-calibration of daily growth increments, stable isotope variation, and temperature in the Gulf of California bivalve mollusk *Chione cortezi*: Implications for paleoenvironmental analysis. Palaios 16: 387-398

Grossman EL, Ku TL (1986) Oxygen and carbon isotope fractionation in biogenic aragonite: Temperature effect. Chem Geol 59:59-74

Jones DS (1981) Annual growth increments in shells of *Spisula solidissima* record marine

temperature variability. Science 211: 165-167

Jones DS, Quitmyer IR (1996) Marking time with bivalve shells: Oxygen isotopes and season of annual increment formation. Palaios 11: 340-346

Jones DS, Thompson I, Ambrose W (1978) Age and growth rate determinations for the Atlantic surf clam *Spisula solidissima* (Bivalvia; Mactracea), based on internal growth lines in shell cross-sections. Mar Biol 47: 63-70

Kaandorp RJG, Vonhof HB, Busto CD, Wesselingh FP, Ganssen GM, Marmol AE, Pittman LR, van Hinte JE (2003) Seasonal stable isotope variations of the modern Amazonian freshwater bivalve *Anodontites trapesialis*. Palaeogeogr Palaeoclimatol Palaeoecol 194: 339-354

Kawahata H, Inoue M, Nohara M, Suzuki A (2006) Stable isotope and chemical composition of pearls: Bimineralization in cultured pearl oysters in Ago Bay, Japan. J Oceanogr 62: 405-412

Kennish MJ (1980) Shell microgrowth analysis. *Mercenaria mercenaria* as a type example for research in population dynamics. In: Rhoads DC and Lutz RA (eds) Skeletal Growth of Aquatic Organisms. Plenum Press, New York: 255-294

Nakashima R, Suzuki A, Watanabe T (2004) Life history of the Pliocene scallop *Fortipecten*, based on oxygen and carbon isotope profiles. Palaeogeogr Palaeoclimatol Palaeoecol 211: 299-307

Tanabe K (1988) Age and growth rate determinations of an intertidal bivalve, *Phacosoma japonicum*, using internal shell increments. Lethaia 21: 231-241

Tanaka N, Monaghan MC, Rye DM (1986) Contribution of metabolic carbon to mollusc and barnacle shell carbonate. Nature 320: 520-523

Urey H (1947) The thermodynamic properties of isotopic substances. J Chem Soc London: 562-581

Wada H (1999) Science for Pearl. Shinju Newspaper Co Ltd., Japan, pp 336 [Japanese]

Weidman CR, Jones DS, Lohmann KC (1994) The long-lived mollusk *Artica islandica*: anew paleoceanographic tool for the reconstruction of bottom temperatures for the continental shelves of the northern North Atlantic Ocean. J Geophys Res 99: 18305-18314

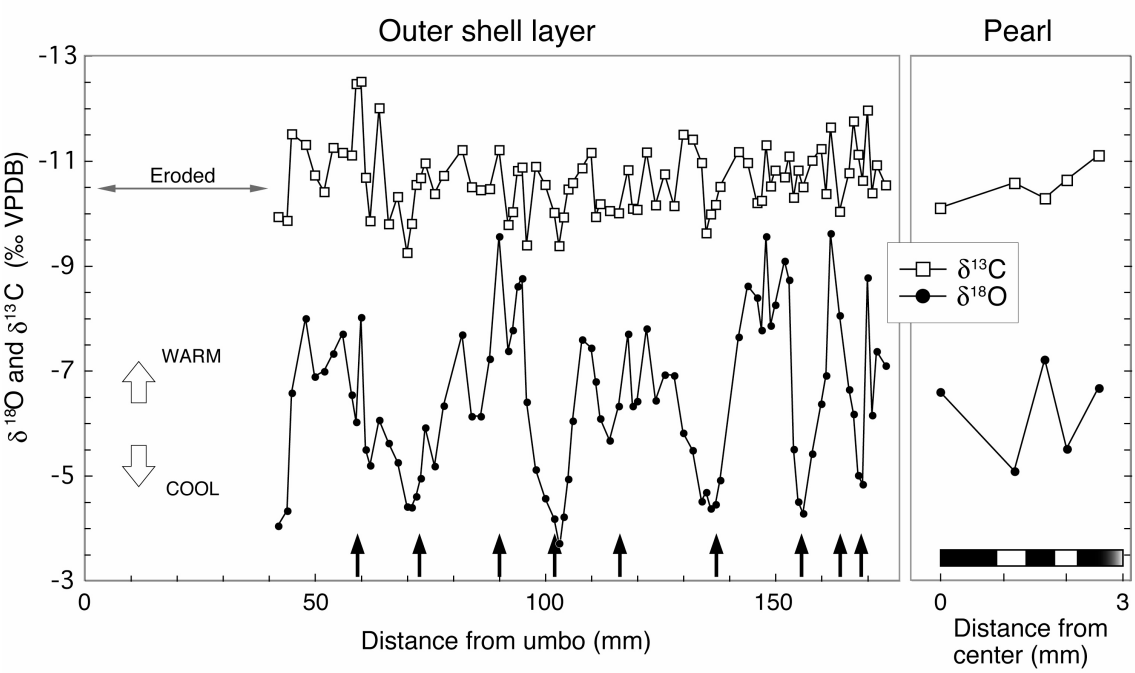

Fig. 1 Oxygen (filled circles) and carbon (open squares) isotope profiles of the outer shell layer and a pearl. Arrows along the bottom of the graph indicate the locations of disturbance rings. The oxygen isotope profile of the outer shell layer showed six cycles. The alternation of bright and dark concentric bands in the pearl is shown in the lower part of the panel

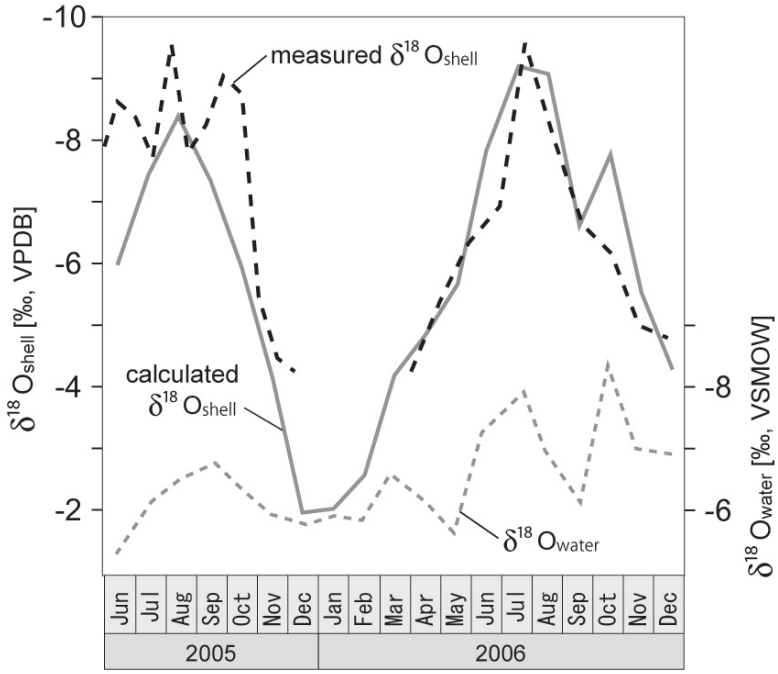

Fig. 2 Comparison of measured $\delta^{18}O_{SHELL}$ data (dashed line) and calculated $\delta^{18}O_{SHELL}$ data (grey solid line). The "calculated $\delta^{18}O_{SHELL}$" were calculated from water temperature and the $\delta^{18}O_{WATER}$ using the equation T (°C) = 20.6 – 4.34($\delta^{18}O_{aragonite}$ – ($\delta^{18}O_{water}$ – 0.2)), after Grossman and Ku (1986) as modified by Goodwin et al. (2001). The water temperature data were taken from observational data at equal interval to the $\delta^{18}O_{WATER}$ data.

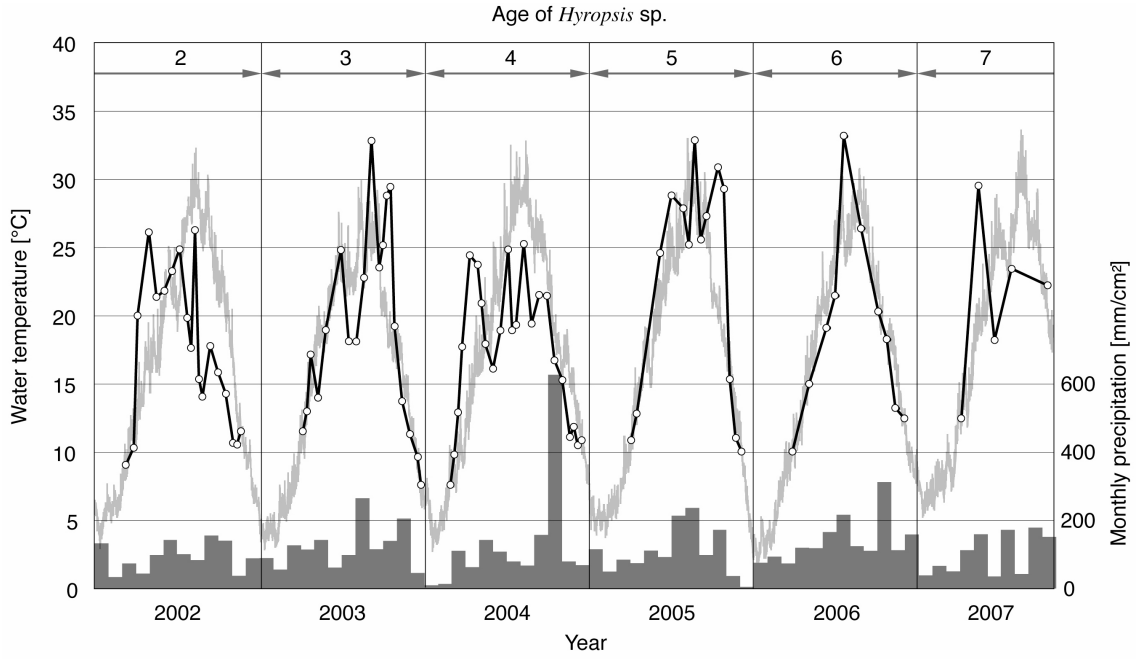

Fig. 3 Comparison of estimated water temperature from the $\delta^{18}O_{SHELL}$ data (open circles) and observed water temperatures (gray line). The histogram shows monthly precipitation. Water temperatures were estimated using the equation T (°C) = 20.6 − 4.34($\delta^{18}O_{aragonite}$ − ($\delta^{18}O_{water}$ − 0.2)), after Grossman and Ku (1986) as modified by Goodwin et al. (2001)

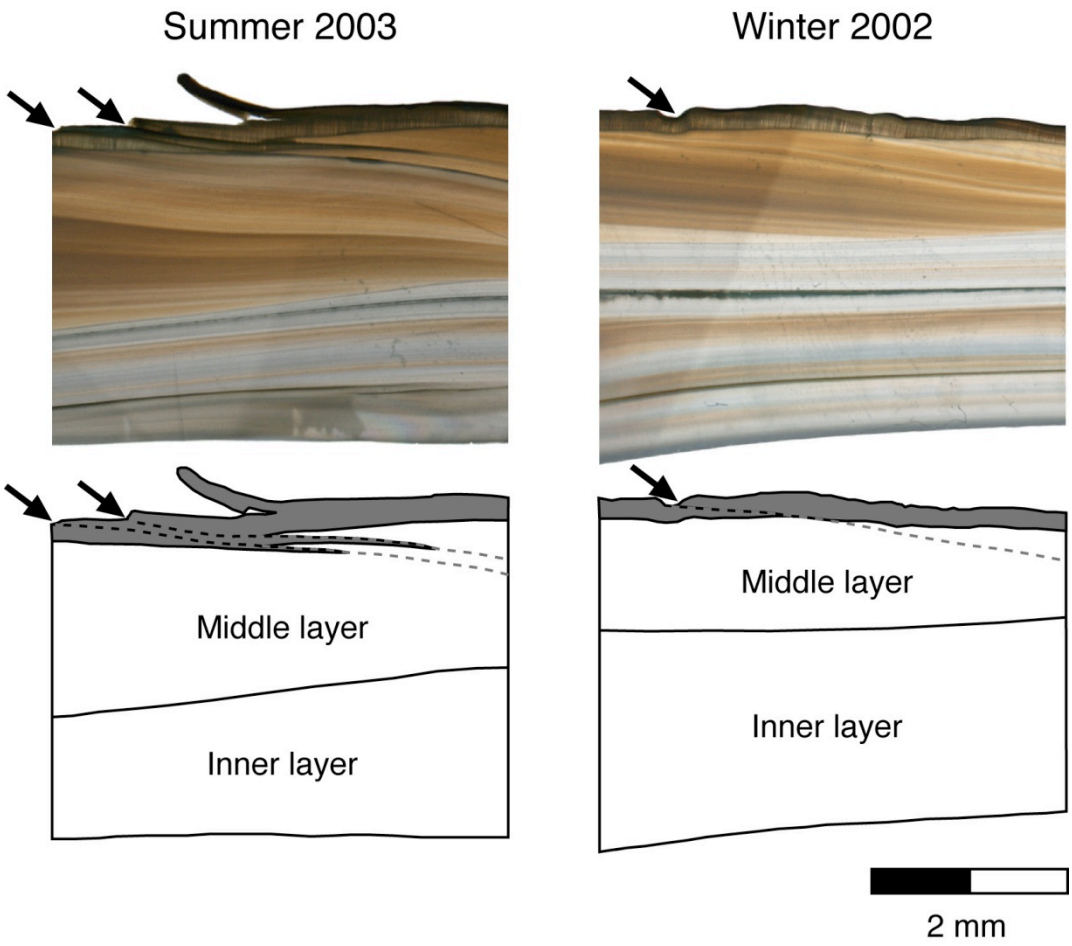

Fig. 4 Photographs of thin sections of the shell and schematic diagrams of the shell structure. The positions of disturbance rings are shown by the black arrows. Structural discontinuities are shown by dashed lines on the schematics. The summer disturbance ring (left) showed a distinct discontinuity at the boundary between the outer and middle shell layers. This structure suggests that the shell formation front retreated by 1–2 mm after growth cessation. Moreover, there were two strong rings in summer 2003. The winter disturbance ring (right) did not show any discontinuity between outer and middle shell layers. Instead, the surface groove was easily traceable from the shell surface to the inner structure

Part Ⅱ: Mg isotope fractionation in hermatypic and deep-sea corals

1 Introduction

Biogenic calcium carbonates of marine organisms have been used for paleoenvironmental reconstruction, such as paleo-water temperature and paleosalinity, under the assumption that stable isotope ratios and elemental ratios of biogenic carbonates are controlled by physiochemical conditions in the ambient water (Urey 1947). A great number of researches have been focused on temperature dependences during isotope/element partitioning of biogenic carbonates because the water temperature is the most fundamental parameter to control earth's surface environment.

Recent developments in mass spectrometers allow exploring new stable isotope systems in cosmochemistry and geochemistry (Halliday et al., 1998; Platzner *et al*., 2008). In the field of paleoceanography, isotope compositions of major and minor constituents of biogenic carbonates such as Ca, Mg and Sr were expected to become new proxies for environmental study. Many researchers have demonstrated Ca isotope analysis on biogenic and inorganic calcium carbonates. The first object of these studies is evaluating the Ca isotopes as a new paleo-thermometer (Zhu and McDougal, 1998). To attempt resolving a temperature dependence of Ca isotope fractionation in biogenic $CaCO_3$, many temperature calibration studies were performed on natural and cultured specimens (e.g., Gussone et al., 2005; 2007; Böhm et al., 2006). These outcomes exhibited small but resolvable temperature dependency on Ca isotope fractionation. In contrast to Ca isotopes, only a few study have reported the Mg isotope composition of skeletal carbonate (Chang et al., 2004; Young and Galy, 2004; deVilliers et al., 2005; Pogge von Strandmann, 2008c). Thus the natural variations of organic/inorganic $CaCO_3$ and the fundamental mechanisms that control the Mg isotope fractionation were poorly understood.

The outcomes of the researches in stable isotopes of the light elements like oxygen and carbon threw a common recognition that biomediated chemical processes obey thermodynamic equilibrium and kinetics (McConaughey, 1989b). Previous works of Ca isotopes suggested some important controlling factors such as crystal lattice structure, physicochemical conditions and biogenic discrimination during Ca isotope fractionations (Gussone et al., 2003; Lemarchand et al., 2004; Böhm et al., 2006). By analogy with Ca isotopes, the difference of mineralogy, physicochemical conditions such as temperature and precipitation rate, and biogenic biases called "vital effects" are expected to be the major controlling factors in the isotope fractionation of Mg isotopes. Multiple genus of planktonic and benthic foraminifera tests indicated that the presence of large vital effects on Mg isotope ratios during Mg incorporations from seawater into calcifying fluids (Chang et al., 2004; Pogge von Strandmann, 2008c). As to the effect of temperature on Mg isotope fractionation, Galy et al. (2002) reported >0.02‰/AMU/ºC of temperature dependence in inorganically precipitated speleothem calcite. In the case of biogenic carbonate, detailed examinations of the relationship

among Mg isotope values, water temperature and shell size indicated that the Mg isotope ratios of foraminifera tests showed no temperature dependence, however (Pogge von Strandmann, 2008c).

Magnesium is a major component in geosphere, biosphere and hydrosphere. In seawater, the concentration of Mg^{2+} is 55mM, and Mg is the 4th major components. The dominant source to the ocean is continental chemical weathering via riverine runoff. The main processes for Mg sinks are hydrothermal alteration of oceanic crusts, limestone dolomitization and ion-exchange reactions of clay minerals. The mean residence time of Mg in modern oceans is approximate 13 million years which is calculated from the riverine inputs (Broecker and Peng, 1982). Therefore, the Mg isotopic composition of the seawater expected to be uniform during at least for several millions years. This long residence time provides advantages for paleoenvironmental reconstructions. It is because the chemical compositions of biogenic carbonate are dependent on both the physicochemical condition and chemical composition of ambient seawaters, and the isotopic and elemental compositions of seawater are changeable through geologic timescale. For example, the isotopic composition of oxygen in the Quaternary seawater had drastically fractionated according to the ice-sheet growth. During the period that Mg isotope value of seawater should remain constant, Mg isotope values of biogenic skeleton is only dependent on the physicochemical condition of ambient seawater and biotic biases. Therefore, Mg isotope ratios of biogenic skeleton are expected to become a new paleo-thermometer during the Quaternary and the Late Tertiary.

In this study, I developed the method for Mg isotope analysis of biogenic $CaCO_3$ and performed high-precision Mg isotope measurements. In order to investigate temperature dependence of Mg isotope fractionation in biogenic $CaCO_3$, the deep-sea corals that collected from various water temperatures were measured. In addition, a possible systematic difference of Mg isotope fractionation was investigated using two major reef dweller, modern and fossil hermatypic corals and fossil giant clam. I here evaluate the plausible controlling factor of Mg isotope fractionation in several biogenic skeletons and present the relationship among Mg isotope values and water temperature and minor and trace elemental concentrations in natural carbonate samples.

2 Materials and methods

2.1 Materials

2.1.1 Deep-sea coral

Deep-sea coral (Precious coral) belongs to Anthozoa Octocorallia. The bathymetric distribution is ranged from several dozen to 2,000m (Iwasaki, 2008). Their skeletons are composed of high-Mg calcite.

Ten specimens of deep-sea coral (*Paracorallium japonicum*, *Corallium elatius*, *C. konjoi*, *Corallium* sp., ?*Keratoisis* sp.) were selected. Sampling localities were Northwest and North Pacific

at water depths of 30-1500m (Fig.5, Table 1). Mean annual water temperatures at sampling localities were taken from Levitus 94 (http://ingrid.ldeo.columbia.edu/SOURCES/.LEVITUS94/). The water temperatures ranged from 2.5 to 19.5ºC (Table 1).

To evaluate the intra-specimen heterogeneity of Mg isotope ratios, subsamples were obtained from *C. elatius* (DPC-0812) and *C. konjoi* (DPC-1). DPC-0812 was cut along the growth axis and sliced into 5-mm-wide thick slabs with a diamond saw. Most part of the skeleton showed red color but the core part only showed white color (Fig. 6). The whitish core part can be traceable along the growth direction. The core part was separated from the reddish outer part using the diamond saw, and the core part was crashed into sand-size with an agate mortar. Then the whitish grains were only picked from among all grains as core part of samples. Both the core part and the outer part were separately powdered in an agate mortar. Moreover, bulk sample was prepared from other part of this specimen. Sample ID of the whitish part, reddish part and bulk were DPC-0812-W, DPC-0812-R and DPC-0812-B, respectively (Fig. 6, Table 1). Two subsamples, DPC-1-23-T1 and DPC-1-KCC, were prepared from distant part of the skeleton of DPC-1 (Table 1). Both subsamples were powdered in an agate mortar.

2.1.2 Hermatypic coral

Hermatypic coral belongs to Anthozoa Hexacorallia. These corals are major constituent of the modern coral reefs that develop in tropical and subtropical shallow waters, typically at depths shallower than 30m.

Massive scleractinian corals, *Porites* sp. and the branching scleractinian corals, *Acropora* sp. were collected for determining Mg isotope fractionation of hermatypic corals. The sampling localities of *Porites* sp. and *Acropora* sp. were Ogasawara and Okinawa-jima, respectively (Fig. 5, Table 1). The fossil hermatypic coral *Porites* sp. was also collected from the Holocene coral terrace of Kikai-jima (Northwest Pacific; 28ºN 129ºW).

The specimens collected living were removed soft tissues, then coral specimens were microsampled by the milling machine at AIST (Advanced Industrial Science and Technology, Japan). Organic materials contained in powdered samples are ordinary removed by chemical treatments, e.g. powdered samples are passed through H_2O_2 and/or $HClO_4$ to decompose organic compounds, in order to minimize interferences on inductivity coupled plasma (ICP) source spectrometry. To evaluate the interference of the organic materials contained in the coral skeletons, I prepared two kinds of powder samples that are with and without organic compounds from the specimen collected from Ogasawara (OGA02-1-1 and OGA02-2-2, Table 1). Each sample was passed through the same column chemistry before Mg isotope measurements.

The two specimens of *Acropora* sp. and fossil *Porites* sp. were cleaned with ultrapure H_2O_2 and distilled water in an ultrasonic bath to remove organic compounds. After chemical treatments, the

branches of each specimen were powdered in an agate mortar.

2.1.3 *Seawater*

To establish the Mg isotopic composition of modern oceans, seawater samples from various localities and depths were analyzed. The seawater samples were collected from the North Sea, North Pacific, East Pacific and Antarctic Sea (Table 1). The water depths of the sampling localities were ranged from 5 to 3,500m.

2.2 Methods

2.2.1 Liquid chromatography

Chemical separation of Mg from $CaCO_3$ and seawater is accomplished by ion exchange method (Chang et al., 2003; Tanimizu, 2008). Following the method of Mg separation for seawater samples described in Tanimizu (2008), I developed a chromatographic method for Mg purification from carbonate samples. The Mg fractions were recovered using a cation exchange resin (AG MP-50; Bio-lad Laboratories, USA). The chemical procedure with 100% recovery of Mg is required, because mass fractionation of Mg isotopes is likely to occur in the chromatographic processes. Carbonate samples contain much higher Ca concentrations compared with seawater samples. This is a crucial problem for Mg isotope analysis because the doubly charged ^{48}Ca cations cause a spectrometric interference on ^{24}Mg. Because the ionization potential of ICP-MS is likely to produce doubly charged Ca ions that potentially make spectral interference in Mg isotope analysis, isobaric $^{48}Ca^{2+}$ interferences can be expected to shift $^{26}Mg/^{24}Mg$ ratios to lower values and to result in showing the mass-independent isotope fractionation on three-isotope plot. In order to validate 100% of Mg separation, 1-5mg of JCp-1 and deep-sea corals were loaded on AG MP-50, and a separate fraction of the eluent was collected at 0.5mL interval during the Mg elution and then analyzed for Mg, Na, K, Ca and Sr contents by ICP-MS (ELAN DRC2). The total amount of alkaline elements, Ca and Sr to the concentration of Mg ([Na+Ca+K+Sr]/[Mg]) was lower than 0.05 (mol ratios). The Mg yield from this method is better than 99%. Carbonate standard JCp-1 (Geological Survey of Japan, AIST, Japan) passed through chemistry yield identical results to unprocessed standards (Table 1). Ca/Mg ratios of purified samples are thus reduced by 5 orders of magnitude relative to unpurified samples, showing effective separation of Mg from the dominant matrix components.

Approximate 5 mg of powdered carbonate sample was weighed in Teflon vials and 0.5mL of 0.6M HCl were added into the vials. Before dissolved samples were loaded on 1mL of cation exchange resin filled in a polypropylene column (40mm length × 5mm in diameter), the resin bed was washed with 6M HCl, and conditioned with 1mL 0.6M HCl prior to loading. Then, sample solutions were loaded on the resin. After 12.5mL of HCl were added in order to separate Mg from other cations (e.g., Na, K, Ca and Sr), the Mg fractions were collected with 5 mL 1.2 M HCl. The

Mg fraction was evaporated to dryness, and a solid $MgCl_2$ was obtained by evaporation of this fraction. These procedures were repeated twice because calcium carbonate samples contain extreme high matrix of Ca, therefore Mg fraction could not be obtained by single purification with a sufficient purity for Mg isotope analysis. After second evaporation, the solid Mg fractions were redissolved in 1mL 0.6M HNO_3. The HCl and HNO_3 used in this study were commercially supplied high-purity TAMAPURE AA-100 reagents (Tama Chemical, Japan). To minimize Mg contamination during chemical preparation, all chemical procedure were carried out in a class-1000 clean room, and class-100 clean benches. Total Mg blank for the two column procedures was less than 3.0ng, which makes $<10^{-3}$ contribution to the sample.

2.2.2 Mg isotope ratio Mass Spectrometry

Mg isotope ratios were measured with a multicollector inductively coupled plasma mass spectrometer (MC-ICP-MS: NEPTUNE Thermo Scientific, Germany) at Center for Advanced Marine Core Research, Kochi University, Japan. Mg isotope measurements were performed by bracketing standard approach (Galy et al., 2001). Standards and samples are prepared as 500ppb Mg solution in 0.15M HNO_3. The differences between the Mg concentration of the standards and samples were kept within 25%, to minimize potential isobaric interferences from matrixes (Galy et al., 2001). The width of the entrance slits before ESA (electrostatic analyzer) was 0.03 mm (medium resolution mode) in order to reduce polyatomic interferences and to reduce signal memory rapidly. The beam intensities for 500ppb Mg solutions were approximately 0.7V for ^{25}Mg. Each run in data acquisition contains 30 scans with an integration time of 4 seconds. The Faraday collectors were set to detect the following isotopes simultaneously: ^{24}Mg (Low3), ^{25}Mg (Center) and ^{26}Mg (High3). Sample solutions were introduced with a 0.1mL/min flow neblizer (Glass Expansion Micromist, Australia) in free aspiration mode attached to dual cyclonic/double Scott glass spray chamber. The results of all samples replicates agree within 100ppm (RSD).

The isotopic data are reported as per mil (‰) deviations relative to seawater reference material IRMM BCR403 (Institute for Reference Materials and Measurements, Belgium). The definition of Mg isotope ratios is:

$$\delta^{x}Mg = \{(^{x}Mg/^{24}Mg)_{sample}/(^{x}Mg/^{24}Mg)_{standard} - 1\} \times 1000 \quad (2)$$

where x refers to either 25 or 26. The Mg solution reagent (Mg-1000, Cica-Reagent) was used for calibration to the seawater scale. I used modern seawater as reference material from the reasons described following. A small isotopic heterogeneity (±0.2‰/AMU) was detected in metal Mg standard reference material NIST SRM980 (Galy et al., 2003) and another metal Mg reference DSM3 showed no SI traceability. A homogeneity of Mg isotopic composition overall oceans had been reported (deVilliers et al., 2005; Tanimizu, 2008; Bolou-Bi et al., 2009). Seawater is suitable for Mg isotopic reference in aspects of availability and isotopic homogeneity under the assumption

that Mg is well isolated from matrix elements with high recovery yield (Tanimizu, 2008). The referenced studies that are reported as other scale like DSM3 and SRM980 were rescaled to seawater scale by the following equation;

$$\delta^{x}Mg_{S\text{-}B} = \{(\delta^{x}Mg_{A\text{-}B} \times 10^{-3} + 1) / (\delta^{x}Mg_{X\text{-}A} \times 10^{-3} + 1) - 1\} \times 10^{3} \quad (3)$$

where S represents sample, and A and B represent different isotope standard materials, and x refers to either 25 or 26.

Three-isotope systematic of Mg (mass numbers 24, 25, and 26 with relative abundance of 78.99, 10.00, and 11.01%) describes clear difference in isotopic partitioning for mass-dependent and mass-independent isotope fractionation. These differences in partitioning are governed by the mass-dependent fractionation laws (Young and Galy, 2004). Giving a definition of a fractionation factor α is defined as:

$$\alpha_{a/b} = (m_2/m_1)_a / (m_2/m_1)_b \quad (4)$$

where a and b refer to two different conditions, and m_2 and m_1 refer to the mass of two different isotopes ($m_2 > m_1$). The relationship among three Mg isotopes in isotope fractionations is:

$$\alpha_{25/24} = (\alpha_{26/24})^{\beta} \quad (5)$$

In the case of terrestrial samples, the exponent β ranged from 0.5110 to 0.5210 (Young et al., 2001b). All $\delta^{26}Mg$ data are on the mass-dependent fractionation line, indicating that there is no significant spectral interference (Fig. 7).

2.2.3 Minor and trace element concentrations

Elemental concentrations of Mg, Ca, Sr, Ba and U were measured with a quadrupole ICP-MS (Hewlett Packard HP-4500) at AIST. Approximate 100 μg of carbonate samples were dissolved in HNO_3. In order to control the instrumental drift and to improve the precision, internal standards (Sc and Y), were added to the solution before digestion by 2% HNO_3. Additionally, standard solutions prepared from JCp-1, a coral standard material provided by geological survey of Japan (GSJ) were measured after every 5th sample for data correction. All element concentrations were given in molar ratio relative to Ca.

3 Results

3.1 Mg isotopic values

3.1.1 Mg isotope values of seawater

The Mg isotope ratios of seawater collected from various depth and locality were ranged between −0.09 and +0.04‰ (Table 2). All measured values were identical within analytical uncertainty. This isotopic homogeneity is consistent with previous works (deVilliers and Nelson, 1999; deVilliers et al., 2005). These observations are consistent with the fact that the major seawater

constituent Mg, which has a quite long residence time of 13 million years in the oceans, are well stirred by the thermohaline circulation. This homogeneity of Mg isotope ratios enables to convert the values of previous works reported as other scales like SRM980 and DSM3 into seawater scales using a equation (3):

$$\delta^{x}Mg_{S\text{-}B} = \{(\delta^{x}Mg_{A\text{-}B} \times 10^{-3} + 1) / (\delta^{x}Mg_{X\text{-}A} \times 10^{-3} + 1) - 1\} \times 10^{3} \quad (3)$$

where S, A and B represent sample, other reference material (SRM980 or DSM3) and seawater, respectively.

3.1.2 Mg isotope values of biogenic carbonates

The Mg isotope values obtained from hermatypic corals, deep-sea corals, and carbonate standard materials (JCp-1, JCt-1) are presented in Fig. 8 and Table 3 with previously reported values of branching hermatypic corals and foraminifera tests (Chang et al., 2004; Pogge von Strandmann, 2008c).

It was shown by several studies that heavier Mg isotopes are depleted in the solid phase relative to liquid phase (Galy et al., 2002; Chang et al., 2004; Buhl et al., 2007; Pogge von Strandmann, 2008c). All Mg isotope values of biogenic $CaCO_3$ also depleted in heavier Mg isotopes relative to seawater. Several biota fractionated Mg isotopes at different magnitude.

The $\delta^{26}Mg$ values of modern hermatypic corals ranged from −0.89 to -0.97‰ (Table 3). All data of branching and massive corals are consistent with the published values of branching hermatypic corals (Chang et al., 2004). The Holocene fossil specimen KKI08-01 also showed identical values to the modern specimens.

Seven species of deep-sea coral had the $\delta^{26}Mg$ values ranging from −2.65 to −2.30‰ (Table 3). Each three and two subsamples prepared from *C. elatius* (DPC-0812) and *C. konjoi* (DPC-1) were identical within analytical uncertainty, although Mg/Ca ratios were slightly differed among subsamples. This indicated that there was no intra-specimen heterogeneity exceeding analytical uncertainty.

The $\delta^{26}Mg$ values in deep-sea corals were positively correlated with ambient water temperatures (Fig. 9). The temperature dependence of Mg isotope fractionation factor α between seawater and deep-sea coral skeletons was represented as the following equation:

$$1000*\ln(\alpha) = -2.68\ (\pm\ 0.04) + 0.0157\ (\pm\ 0.0030)*T\ (^{\circ}C) \quad (6)$$

3.2 Minor and trace element concentrations

The obtained minor and trace elemental concentrations of specimens were listed in Table 3. The Mg/Ca ratios of the deep-sea corals ranged from 73.75 to 137.40mmol/mol (Table 3). The relationship between temperature and Mg/Ca ratios in deep-sea corals is given in Fig. 10. The obtained Mg/Ca values clearly increased with increase of water temperature, showed clear positive

correlation with water temperatures. This increase in Mg/Ca ratios with increasing water temperature corresponds with published data of deep-sea corals (Weinbauer et al., 2000; Bond et al., 2005; Iwasaki 2008). The obtained regression equation of this study was very similar to the previously reported equation of *C. rubrum* (Weinbauer et al., 2000). This positive correlation between water temperature and Mg/Ca ratios is consistent with inorganically precipitated calcite and the other species of deep-sea coral and benthic foraminifera, which have the skeletal mineralogy of high-Mg calcite. In contrast to the Mg/Ca ratio, the Sr, Ba and U elemental concentrations of deep-sea corals showed no correlation with temperature.

4 Discussion

4.1 Isotopic fractionation mechanisms in $CaCO_3$

The results of this study and previous studies showed remarkable inter-taxon variability in $\delta^{26}Mg$. In order to discuss the difference of Mg isotope fractionation in biogenic skeletons, I enumerate the possible controlling factors from the previous works on biogenic and inorganic $CaCO_3$.

The elemental concentrations in $CaCO_3$ have been used as a reliable paleo-thermometer (McCulloch et al., 1994; Felis et al., 2004). In general, substitutions of Mg for Ca in $CaCO_3$ are governed by equilibrium-based thermodynamic partitioning or kinetically controlled inorganic partitioning (Kinsman and Holland, 1969; Gaetani and Cohen, 2006). Calcite, one of the $CaCO_3$ polymorph, is classified into low-Mg calcite and high-Mg calcite according to the Mg content. Low-Mg calcite can be precipitated only from solutions where its Mg/Ca ratios is <0.1; in contrast the Mg/Ca ratios of seawater is 5.14 (Mucci and Morse, 1983). Since the presence of Mg^{2+} in the fluid is known to inhibit crystal formation of calcite (Mucci and Morse, 1983; Davis et al, 2000; Zeebe and Sanyal, 2002), particular biota (e.g., brachiopods and planktonic foraminifera) are thought to make an effort to reduce the Mg/Ca ratios in calcifying solutions in order to have an advantage in calcification (Rosenheim et al., 2005).

Because Mg is incorporated into $CaCO_3$ by ion substitution of calcium, Mg isotopic fractionations are assumed to be governed by physicochemical processes that are common to Ca isotope fractionation. Strontium is another major-minor element of $CaCO_3$, and its isotope fractionation of inorganic aragonite and hermatypic corals indicated the similarity of isotope fractionation mechanisms between Sr and Ca (Fietzke and Eisenhauer, 2006). According to the isotope fractionation model of calcium, there are several important factors controlling isotopic fractionation in $CaCO_3$ precipitation. First of all, the isotope fractionation effects are greatly differed from the systematic in traditional isotopes like oxygen and carbon isotopes. The isotope fractionation of carbon and oxygen in $CaCO_3$ is mainly controlled by the vibrational behavior of the C-O covalent bond (Urey, 1947; Sakai and Matsuhisa, 1996). Based on this property, oxygen isotope fractionation

shows a clear temperature dependence, and has been used for paleoenvironmental reconstruction as paleothermometer. (e.g., Epstein et al., 1953). In contrast, dominant bond character of cations such as Ca, Mg and Sr in $CaCO_3$ is ionic. The behavior of ionic bond during isotopic fractionation is still controversial. The bond energy of the Ca-O bond in $CaCO_3$ is four times weaker than that of the C-O bond and the covalent contribution to the bond energy is 20.6% (Reeder, 1983). Therefore, isotope fractionation coefficients between two polymorphs of $CaCO_3$ (calcite and aragonite) are expected to be small (O'Neil, 1986). However, Gussone et al. (2003) observed a resolvable difference between calcite and aragonite, indicating that Ca isotope fractionation in biogenic and inorganic $CaCO_3$ is influenced by the crystal lattice structure. Moreover, Gussone et al. (2005) suggested that the underlying mechanism for this offset between calcite and aragonite may be related to the different coordination numbers and bond strengths of the Ca ions, or to different Ca reaction behavior at the solid-liquid interface. Gussone et al. (2003) also suggested that the observed Ca isotope fractionation was controlled by a kinetic isotope effect. Their model explained that two different slopes of temperature dependence on Ca isotope fractionation observed in foraminifera species and inorganic calcite were caused by the existence or nonexistence of aquocomplexes for diffusive Ca in aqueous solution. On the other hand, Marriot et al. (2004) suggested Ca isotopes are fractionated at isotopic equilibrium condition. Lemarchand et al. (2004) suggested the precipitation rate of $CaCO_3$ largely affect on isotope fractionation. In their model, heavy Ca isotopes dissolved in aqueous solution are incorporated into solid phase due to the expansion of ion exchange layer between solid $CaCO_3$ and bulk aqueous solution. Several study suggest that a vital effect are remarkable during Ca uptake from seawater (e.g., Böhm et al., 2006).

4.2 Mg isotope fractionation during biomineralization process

It was shown by several studies that heavier Mg isotopes are depleted in the solid phase relative to seawater (Galy et al., 2002; Chang et al., 2004; Buhl et al., 2007; Pogge von Strandmann, 2008c). According to the Ca isotope fractionation, the difference of mineralogy, physicochemical conditions such as temperature and precipitation rate are expected to be major controlling factor of Mg isotope fractionation in biogenic and inorganic $CaCO_3$. As to mineralogy, the difference of isotope fractionation between two $CaCO_3$ polymorphs is possibly owing to the different coordination numbers and bond strengths, or to different reaction behavior at the solid-liquid interference (Gussone et al., 2005). With an increase of precipitation rates, unfractionated heavy isotopes are incorporated into solid phase (Lemarchand et al., 2004). This effect is explained by the expansion of the interface layer between the fluid and growing crystal. Thus, higher calcification rates cause less isotope fractionation between solution and crystal.

Furthermore, the concentrations of two major "minor element", Mg and Sr substituting for Ca into biogenic carbonate varied greatly among different taxon. In theory, distribution coefficients of

minor elements in calcium carbonates are strongly controlled by the lattice structure (Zeebe and Sanyal, 2002). Two polymorphs of $CaCO_3$, calcite and aragonite, are hexagonal and orthorhombic system, respectively. Calcite preferentially incorporates small divalent cations like Mg, Fe and Mn, and aragonite incorporate larger cations like Sr, Pb and Ba. Typical concentrations of minor elements in inorganically precipitated calcite and aragonite are showed in Fig. 11 (Reeder, 1990). The Mg/Ca and Sr/Ca ratios of hermatypic corals and inorganic aragonite are reported to be within similar ranges (Fig. 11, Chang et al., 2004; Rosenheim et al., 2005). Erez et al. (2002) reported that scleractinian coral skeletons are grown in an aqueous solution whose composition is close to the seawater and the controlling factors during aragonite precipitation are close to inorganic process. The skeletons of deep-sea corals are composed of high-Mg calcite. The Mg/Ca of deep-sea corals ranged from 73 to 121mmol/mol. The distribution coefficient of Mg of deep-sea corals also showed similar values to inorganic calcite precipitated under equilibrium condition (Fig. 11, Mucci, 1987; Burton and Walter, 1991; Reeder, 1990; Dietzel et al., 2004). Moreover, the Mg/Ca ratios of the deep-sea corals are positively correlated with annual mean water temperature. This positive correlation between temperature and the D_{Mg} are commonly observed in inorganically/biogenically precipitated calcite and aragonite. The slope of temperature dependence of deep-sea corals is identically similar to inorganic calcite. From the results of Mg concentrations and the temperature dependence on Mg distribution, the calcification process of deep-sea corals is rather close to inorganic process than strong biologically mediated process.

As to δ^{26}Mg values, two genus of hermatypic corals (*Acropora* sp. and *Porites* sp.) showed δ^{26}Mg values in the same range as previously published values of inorganically precipitated aragonite (Chang et al., 2004). Also, deep-sea corals exhibited same magnitude of isotope fractionation (-2.5‰) to the fractionation coefficient between the inorganically precipitated speleothem calcite and ground water (-2.7‰; Galy et al., 2002). Combined with the results of Mg/Ca ratios, the possible explanation for these observations is the presence of strong mineralogical control on Mg isotope fractionation. Even though the precipitation rates of both corals were much higher than natural inorganic precipitates, these corals had δ^{26}Mg values equivalent to abiotic aragonite and calcite. This may indicates that the different coordination numbers and bond strengths or to different reaction behavior at the solid-liquid interface largely influenced on Mg isotope fractionation. For further understanding, more data are required on Mg isotope fractionation during both biogenic and inorganic calcification.

Both scleractinian hermatypic corals and shells of giant clam (carbonate reference material JCt-1) are also composed of aragonite. These are both reef dweller, and their habitat environments are almost identical. Although the logarithm of calcification ratios, R [μmol/m^2/h] of both genus are approximately 5 (Böhm *et al*., 2006; Watanabe *et al*., 2004), these two taxon showed large difference in δ^{26}Mg values (Fig. 8). Giant clams showed 1.5‰ lighter values relative to hermatypic corals.

Moreover, Mg/Ca and Sr/Ca ratios of aragonitic bivalve shells are lower compared to hermatypic corals and inorganic aragonite (Fig. 12). The Mg/Ca and Sr/Ca ratios of giant clam (JCt-1) sample are one thirds and one fifths, respectively (Okai et al., 2004). In the case of planktonic foraminifera, shells are composed of low-Mg calcite. In contrast to the coral aragonite and high-Mg calcite, the biogenic discrimination are remarkable on Mg uptake during ion transport process from seawater to calcifying fluids. The correlation between δ^{26}Mg values and Mg/Ca ratios indicated that foraminifera tests showed no-significant tendency between them in contrast to deep-sea corals (Fig. 12). The discrepancies between foraminifera and deep-sea corals may support the presence of large vital effect in foraminifera tests and the similarity of Mg isotope fractionations between deep-sea corals and speleothem calcite. Given the fact that both mineralogy and precipitation rates are not the cause of the differences between hermatypic corals and giant clam, most plausible explanation for the Mg isotope difference of biogenic carbonates is vital effects accompanied with active controls of chemical compositions of their calcifying fluids. As shown above, the giant clam and the foraminifera showed lower values in δ^{26}Mg relative to hermatypic and deep-sea corals (Fig. 8). Low-Mg calcite of giant clam and foraminifera are thought to precipitate from the Mg-depleted calcifying fluids accomplished by the biotic controls (Mucci, 1987). Both of the biological fractionations observed in aragonite and calcite skeletons are enriched in the light Mg isotopes. Therefore, a large isotope fractionation may have been occurred during the Mg transport process from seawater to calcifying fluids.

4.3 Temperature dependence of Mg isotope fractionation in Deep-sea coral

The present study showed a clear negative temperature-dependence of Mg isotope fractionation (Fig. 9). The obtained regression equation for the deep-sea corals is:

$$1000*\ln(\alpha) = -2.68\ (\pm\ 0.04) + 0.0157\ (\pm\ 0.0030)*T\ (^{\circ}\mathrm{C}) \quad (6)$$

The negative correlations between temperature and isotope fractionation of divalent cations have been demonstrated in Ca and Sr isotope fractionations of biotic and abiotic $CaCO_3$ (e.g. Näglar *et al.*, 2000; Gussone *et al*., 2003; Böhm *et al*., 2006 Fietzke and Eisenhauer, 2006). A Recent model predicted that increase in temperature induces higher diffusivity of heavy isotopes and a decreases isotope fractionation (Tang *et al*., 2008b). Galy et al. (2002) showed a temperature dependence of isotope fractionations in speleothems precipitated from groundwater. The difference of δ^{26}Mg between speleothems and drip waters was ~2.7‰ and the temperature dependence is less than 0.02 ‰/AMU/ºC in the temperature range from 4 to 18ºC, resulting in ~0.0075‰/AMU/ºC in the temperature range from 20 to 30 ºC (Galy et al., 2002; Pogge von Strandmann, 2008c). The Mg isotope fractionation of speleothem was similar to that of deep-sea corals with respect to the degree of isotope fractionation and its temperature dependence. This implicated that Mg isotope fractionations of both speleothem and deep-sea corals were controlled by the common mechanisms.

Previous studies reported distinct slopes on temperature dependence of Ca and Sr isotope fractionation (Nägler et al., 2000; Gussone et al., 2003; Fietzke and Eisenhauer, 2006). The difference of the slopes can be interpreted as the presence of aquocomplexes with large hydration numbers. Taking into the account of relative mass difference of Mg isotopes and vibrational energy of Mg-O bond, the observed slope did not corresponded to the steeper slopes of Ca and Sr isotopes fractionation.

On the other hand, in the case of planktonic foraminifera, there is no obvious temperature dependence on Mg isotope fractionation, however (Chang et al., 2004). A recent study using the high-precision Mg isotope measurements also showed no resolvable temperature dependence is observed (Pogge von Strandmann, 2008c). A numerical model study represents variations of temperature dependence on Ca isotope fractionation during inorganic calcite formation is varied according to the effect of precipitation rates (Tang et al, 2008b). The precipitation rate of planktonic foraminifera species is known to demonstrate rapid calcification that is 2 orders larger than that of deep-sea corals (Iwasaki, 2008). The difference of the precipitation rates may affect the temperature dependence of biogenic $CaCO_3$.

Deep-sea corals had weak but resolvable temperature dependence on Mg isotope fractionation. This temperature dependence suggests the possible availabilities of Mg isotopes in biogenic $CaCO_3$ as new paleotemperature proxy. This is potentially more robust to the short-term fractionations of seawater composition.

5 Conclusions

High precision Mg isotope analysis technique on modern and fossil biogenic $CaCO_3$ was developed. Heavier Mg isotopes were depleted in biogenic skeletons relative to seawater. Hermatypic and deep-sea corals were lower in $\delta^{26}Mg$ values by 1.0 and 2.5 ‰ compared with seawater, respectively. The results of $\delta^{26}Mg$ values of hermatypic corals showed isotope fractionation coefficients were consistent with previously reported values. $\delta^{26}Mg$ values of hermatypic and deep-sea corals showed similar values to the inorganically precipitated aragonite and calcite. $\delta^{26}Mg$ values of giant clam was -2.58‰. Giant clam was more depleted in heavy isotopes relative to hermatypic corals. Taking elemental partitioning of Mg of giant clams into consideration, both mineralogy and precipitation rate is not the main factor controlling the large isotope fractionation of giant clam. Given the fact that their shells are precipitated from closed and biologically controlled systems as to Mg concentrations, the plausible explanation for this large isotope fractionation is vital effects during the Mg uptake from seawater into calcifying fluids. Moreover, clear temperature dependence of Mg isotope fractionation was observed in deep-sea corals. The obtained slope (0.0078‰/°C/AMU) is similar to that of the inorganically precipitated

calcite speleothem (Galy et al., 2002). The Mg concentrations and the relationship between Mg/Ca and temperature of deep-sea corals were also plotted on the same range and the regression line of inorganically precipitated calcite. These consistency between inorganic and deep-sea corals is possibly the result of strong mineralogical control on Mg isotope fractionation. The obtained temperature dependence of Mg isotope fractionation in biogenic $CaCO_3$ implies Mg isotopes as new environmental proxy for water temperature.

6 Acknowledgements

I express the first appreciation to my supervisor, professor Hodaka Kawahata for overall support. I also express my appreciation to Dr. Masaharu Tanimizu of JAMSTEC for many instructions of chemical preparations and instrumental analysis, helpful comments, valuable discussions, thoughtful reviews and many supports. Special thanks to Dr. Atsushi Suzuki of AIST for instructing the foundations of researches, supports for experiments and providing the thoughtful comments and advises, to professor Nozomu Iwasaki of Kochi University for providing the specimens and valuable advises, and to Dr. Mayuri Inoue of ORI for overall support and constructive comments. My master thesis is benefited from many helps by Dr. Tsuyoshi Ishikawa of JAMSTEC, Dr. Rei Nakashima and of AIST, Dr. Atsushi Matsuoka and Dr. Kazuya Nagaishi of Marine Work Japan, Ms. Hiroko Hashizume of KCC, Dr. Azumi Kuroyanagi, Ms. Kyoko Yamaoka, Mr. Hiroyuki Ushie, Ms. Natsumi Hokanishi, Ms. Yumiko Yoshinaga, Ms. Kyoko Koda and my colleagues.

7 References

Böhm, F., Gussone, N., Eisenhauer, A., Dullo, W.-C., Reynaud, S., Payton, A., 2006. Calcium isotope fractionation in modern scleractian corals. Geochim. Cosmochim, Acta 70, 4452-4462.

Bolou-Bi, E.B., Vigier, N., Brenot, A., Poszwa, A., 2009, Magnesium Isotope Compositions of Natural Reference Materials. Geostand. Geoanal. Res. 33, 95-109.

Bond, Z.A., Cohen, A.L., Smith, S.R., Jenkins, W.J., 2005, Growth and composition of high-Mg calcite in the skeleton of a Bermudian gorgonian (*Plexaurella dichotoma*): Potential for paleothermometry. Geochem. Geophys. Geosys. doi:10.1029/2005GC000911.

Broecker, W.S., Peng, T.-H., 1982, Tracers in the Sea. Eldigo Press, Palisades, NY.

Burton, E.A., Walter, L.M., 1991. The effects of PCO_2 and temperature on magnesium incorporation in calcite in seawater and $MgC1_2$–$CaCl_2$ solutions, Geochim. Cosmochem. Acta 55, 777–785.

Buhl, D., Immenhauser, A., Smeulders, G., Kabiri, L., Richter, D.K., 2007. Time series $\delta^{26}Mg$ analysis in speleothem calcite: Kinetic versus equilibrium fractionation, comparison with other proxies and implications for palaeoclimate research. Chem. Geol. 244, 715–729.

Carpenter, S.J., Lohmann, K.C., 1992. Sr/Mg ratios of modern marine calcite: empirical indicators of ocean chemistry and precipitation rate. Geochim. Cosmochim. Acta 56, 1837–1849.

Chang, V.T.-C., Makishima, A., Belshaw, N.S., O'Nions R.K., 2003. Purification of Mg from low-Mg biogenic carbonates for isotope ratio determination using multiple collector ICP-MS, J. Anal. At. Spectrom. 18, 296–301.

Chang, T.C., Williams, R.J.P., Makishima, A., Belshawl, N.S., O'Nions, R.K., 2004. Mg and Ca isotope fractionation during $CaCO_3$ biomineralization. Biochem. Biophys. Res. Comm. 323, 79-85.

Davis, K.J., Dove, P.M., De Yereo, J.J., 2000. The role of Mg^{2+} as an impurity in calcite growth. Science 290, 1134-1137.

de Villiers, S., Nelson, B.K., 1999. Detection of low-temperature hydrothermal fluxes by seawater Mg and Ca anomalies. Science 285, 721– 723.

de Villiers, S., Dickson, J.A.D., Ellam, R.M., 2005. The composition of the continental river weathering flux deduced from seawater Mg isotopes. Chem. Geol. 216, 133-142.

Dietzel, M., Gussone, N., Eisenhauer, A., 2004. Co-precipitation of Sr^{2+} and Ba^{2+} with aragonite by membrane diffusion of CO_2 between 10 and 50 °C. Chem. Geol. 203, 139–151.

Epstein S.R., Buchsbaum R., Lowentein H.A., Urey H.C., 1953. Revised carbonate-water isotopic temperature scale. Geol. Soc. Am. Bull. 64, 1315-1326.

Erez, J., Bentov, S., Brownlee, C., Raz, M., Rinkevich, B., 2002. Biomineralisation mechanisms in foraminifera and coral and their paleoceanographic implications, Geochim. Cosmochem. Acta 1 (66/S) A216.

Felis, T., Lohmann, G., Kuhnert, H., Lorenz,S. J., Scholz, D., Patzold, J., Al-Rousan, S.A., Al-Moghrabi, S.M., 2004. Increased seasonality in Middle East temperatures during the last interglacial period, Nature 429, 164–168.

Fietzke, J., Eisenhauer, A., 2006. Determination of temperature-dependent stable strontium isotope ($^{88}Sr/^{86}Sr$) fractionation via bracketing standard MC-ICP-MS. Geochem. Geophy. Geosys. 7, Q08009, doi:10.1029/2006GC001243.

Gaetani, G.A., Cohen, A.L., 2006. Element partitioning during precipitation of aragonite from seawater: A framework for understanding paleoproxies. Geochim. Cosmochim. Acta 70, 4617-4634.

Galy, A., Belshaw, N.S., Halicz, L., O'Nions, R.K., 2001. High-precision measurement of magnesium isotopes by multiple-collector inductively coupled plasma mass spectrometry. Int. Jour. Mass Spectrometry 208, 89 –98.

Galy, A., Bar-Matthews, M., Halicz, L., O'Nions, R.K., 2002. Mg isotopic composition of carbonate: insight from speleothem formation. Earth Planet. Sci. Lett. 201, 105-115.

Galy, A., Yoffie, O., Janney, P.E., Williams, R.W. Cloquet, C., Alard, O., Haliz, L., Wadhwa, M., Hutcheon, I.D., Ramon, E., Carignan, J., 2003. Magnesium isotope heterogeneity of the isotopic standard SRM980 and new reference materials for magnesium-isotope-ratio measurements. Jour. Anal. At. Spectrum. 18, 1352-1356.

Gussone, N., Eisenhauer, A., Heuser, A., Dietzel, M., Bock, B., Böhm, F., Spero, H. J., Lea, D. W., Bijma, J., Nagler, F., 2003. Model for kinetic effects on calcium isotope fractionation ($\delta^{44}Ca$) in inorganic aragonite and cultured planktonic firaminifera. Geochim. Cosmochim. Acta 67, 1375-1382.

Gussone, N., Böhm, F., Eisenhauer, A., Dietzel,M., Heuser, A., Teichert, B.M.A., Reitner, J., Worheide, G., Dullo,W.C., 2005. Calcium isotope fractionation in calcite and aragonite. Geochim. Cosmochim. Acta 69, 4485–4494.

Gussone, N., Langer, G., Geisen, M., Steel, B. A., Riebesell, U., 2007. Calcium isotope fractionation in coccoliths of cultured Calcidiscus leptoporus, Helicosphaera carteri, Syracosphaera pulchra and Umbilicosphaera foliosa. Earth Planet. Sci. Lett. 260, 505–515.

Halliday, A.N., Lee, D.-C., Christensen, J.N., Rehkämper, M., Yi, W., Luo, X., Hall, C.M., Ballentine, C. J., Pettke, T., Stirling. C., 1998. Applications of Multiple Collector-ICPMS to Cosmochemistry, Geochemistry, and Paleoceanography. Geochim. Cosmochim. Acta 62, 919-940.

Iwasaki, N. eds., 2008. Biohistory of precious corals. Tokai University Press, 364 pp (Japanese)

Kinman, D.J.J., Holland, H.D., 1969. The coprecipitation of cations with with $CaCO_3$; 4. The coprecipitation of Sr^{2+} with aragonite between 16 and 96 °C. Geochim. Cosmochem. Acta 33, 1–17.

Lemarchand, D., Wasserburg, G.J., Papanastassiou, D.A., 2004. Rate-controlled calcium isotope fractionation in synthetic calcite. Geochim. Cosmochim. Acta 68, 4665-4678.

Marriott, C.S., Henderson, G.M., Belshaw, N.S., Tudhope, A.W., 2004. Temperature dependence of $\delta^{7}Li$, $\delta^{44}Ca$ and Li/Ca during growth of calcium carbonate. Earth Planet. Sci. Lett. 222, 615–624.

McConnaughey T., 1989b. ^{13}C and ^{18}O isotopic disequilibrium in biological carbonate: II. In vitro simulation of kinetic isotope effects. Geochim. Cosmochim. Acta 53, 163–171.

McCulloch, M.T., Gagan, M.K., Mortimer, G.E., Chivas, A.R., Isdale P.J., 1994. A high-resolution Sr/Ca and $\delta^{18}O$ coral record from the Great Barrier Reef, Australia, and the 1982–1983 El Nino, Geochim. Cosmochim. Acta 12, 2747–2754.

Mucci, A., Morse, J.W., 1983. The incorporation of Mg^{2+} and Sr^{2+} into calcite overgrowths: influences of growth rate and solution composition. Geochim. Cosmichem. Acta 47, 217–233.

Mucci, A., 1987. Influence of temperature on the composition of magnesium calcite overgrowths precipitated from seawater, Geochim. Cosmochem. Acta 51, 1977–1984.

Näglar, T.F., Eisenhauer, A., Muller, A., Hemleben, C., Kramers, J., 2000. The δ^{44}Ca-temperature calibration on fossil and cultured *Globigerinoides sacculifer*: New tool for reconstruction of past sea surface temperature. Geochem. Geophys. Geosys. 1, doi:10.1029/2000GC000091.

Okai, T., Suzuki, A., Terashima, S., Inoue, M., Nohara, M., Kawahata, H., Imai, N., 2004. Collaborative analysis of GSJ/AIST geochemical reference materials JCp 1 (Coral) and JCt 1 (Giant Clam). Geochemistry 38, 281-286. (in Japanese)

O'Neil, J.R., 1986. Theoretical and experimental aspects of isotope fractionation. Rev. Mineral. 16, 1-40.

Platzner, T.I., Segal, I., Halicz, L., 2008. Selected isotope ratio measurement of light metallic elements (Li, Mg, Ca, and Cu) by multiple collector ICP-MS. Anal. Bioanal. Chem. 390, 441-450.

Pogge von Strandmann, P.A.E., 2008c. Precise magnesium isotope measurements in core top planktic and benthic foraminifera. Geochem. Geophys. Geosys. 9, Q12015, doi:10.1029/2008GC002209.

Reeder, R.J. eds., 1990. Carbonates: Mineralogy and Chemistry, Reviews in Mineralogy, 11. Mineralogical Society of America, Washington, DC. 399 pp.

Rosenheim, B.E., Swart, P.K., Thorrold, S.R., 2005. Minor and trace elements in sclerosponge Ceratoporella nicholsoni: Biogenic aragonite near the inorganic endmember?. Palaeogeogr. Palaeoclimatol. Palaeoecol. 228, 109–129

Sakai, H., Matsuhisa, Y., 1996. Stable isotope geochemistry. University of Tokyo Press, 403 pp. (in Japanese)

Steuber, T., 1999. Isotopic and chemical intra-shell variations in low-Mg calcite of rudist bivalves (Mollusca: *Hippuritacea*): disequilibrium fractionations and Late Cretaceous seasonality. Int. J. Earth Sci. 88, 551–570.

Tanimizu, M., 2008. Determination of Mg isotopic composition of seawater with rapid Mg purification. J. Nucl. Sci. Tech. Supp6, 51-54.

Tang, J., Dietzel, M., Böhm, F., Köhler, S.J., Eisenhauer A., 2008. Sr^{2+}/Ca^{2+} and $^{44}Ca/^{40}Ca$ fractionation during inorganic calcite formation: II. Ca isotopes. Geochim. Cosmochim. Acta 72, 3733–3745.

Urey, H., 1947. The thermodynamic properties of isotopic substances. J. Chem. Soc. London 562-581.

Watanabe, T., Suzuki, A., Kawahata, H., Kan, H., Ogawa, S. 2004. A 60-year isotopic record from a mid-Holocene fossil giant clam (*Tridacna gigas*) in the Ryukyu Islands: physiological and paleoclimatic implications. Palaeogeogr. Palaeoclimatol. Palaeoecol. 212, 343-354.

Weinbauer, M.G., Brandstatter, F., Velimirov, B., 2000, On the potential use of magnesium and strontium concentrations as ecological indicators in the calcite skeleton of the red coral (*Corallium rubrum*), Mar. Biol.,137, 801–809.

Young, E.D., Galy, A., Nagahara, H., 2001b. Kinetic and equilibrium mass-dependent isotope fractionation laws in nature and their geochemical and cosmochemical significance. Geochim. Cosmochim. Acta 66, 1095–1104.

Young, E.D., Galy, A., 2004. The isotope geochemistry and cosmochemistry of magnesium, in: C.M. Johnson, B. B.L., F. Albarede, (eds.), Geochemistry of nontraditional stable isotopes, Reviews in Mineralogy and Geochemistry 55, Mineralogical Society of America, Geochemical Society.

Zeebe, R.E., Sanyal, A., 2002. Comparison of two potential strategies of planktonic foraminifera for house building: Mg^{2+} or $H^{\cdot}$ removal? Geochim. Cosmochim. Acta 66, 1159–1169.

Zhu, P., Macdougall, J.D., 1998. Calcium isotopes in the marine environment and the oceanic calcium cycle. Geochim. Cosmochim. Acta 62, 1691–1698.

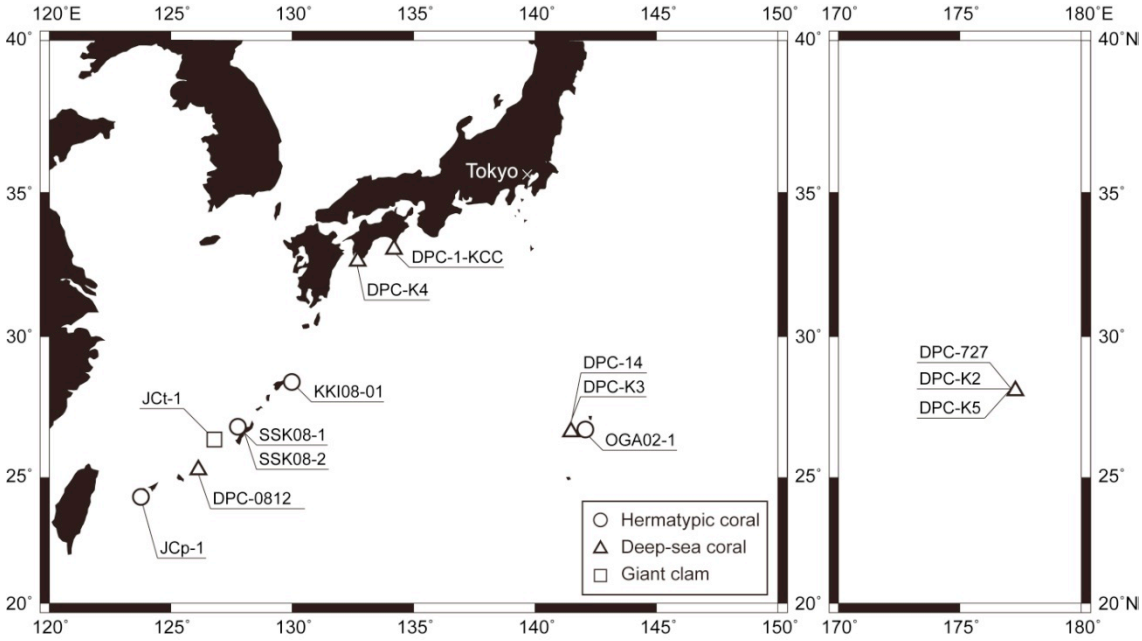

Fig. 5 Map showing the approximate location of sampling point of the specimen. The circles indicate the sampling localities of hermatypic corals, the triangles are deep-sea corals, and the square is fossil giant clam.

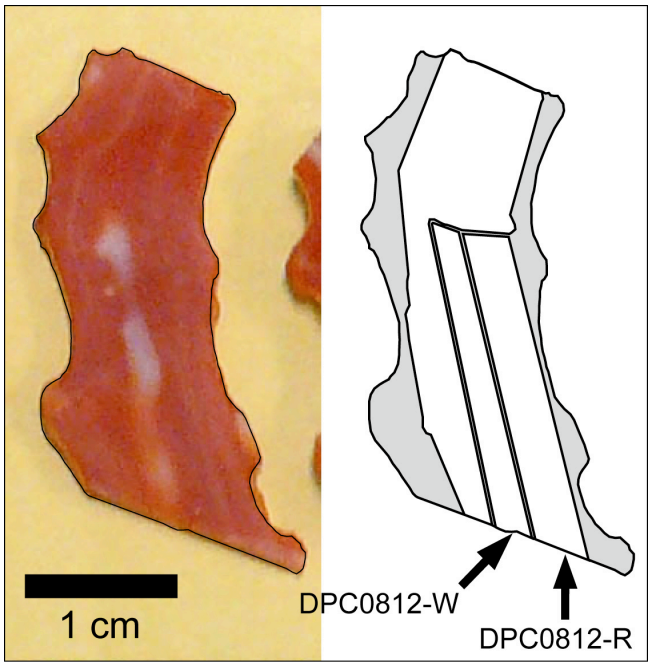

Fig. 6 Photograph and schematic of cross section of the deep-sea coral *Corallium elatius* (DPC-0812-W and DPC-0812-R). The core part only showed white color. Right schematic shows cutting method of core part apart from the reddish outer part. The core part was crashed into sand-size with an agate mortar, then the whitish grains were only picked from among all grains as core part of samples.

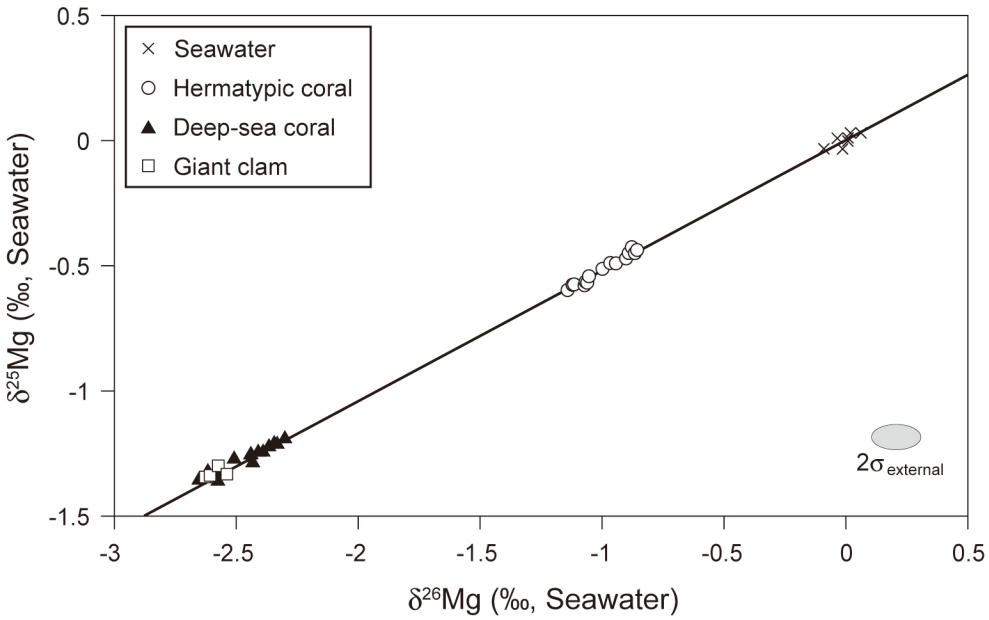

Fig. 7 Three isotope plot of Mg isotopes expressed in δ-unit in the seawater scale. The solid line corresponds to the mass-dependent fractionation line.

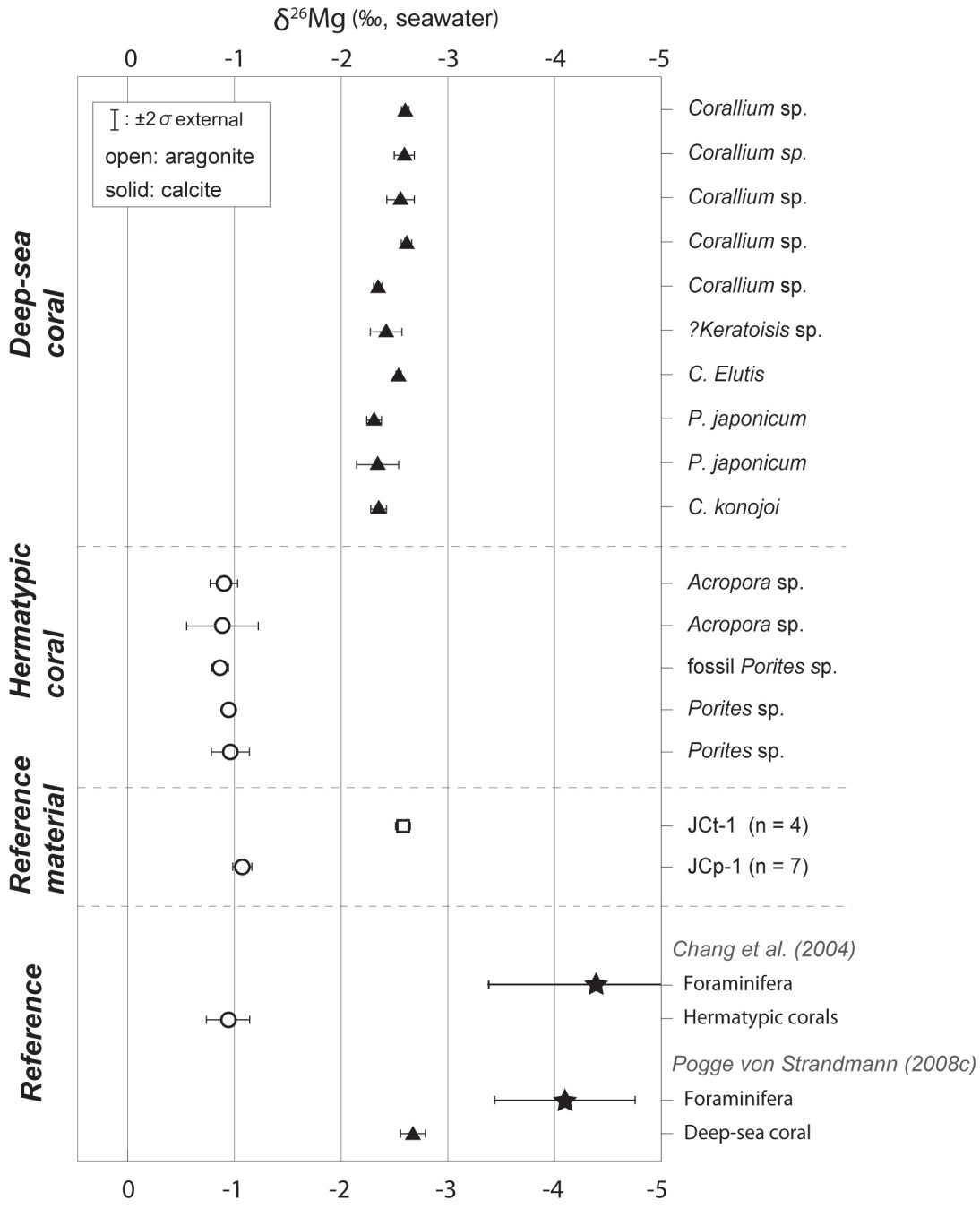

Fig. 8 Range of measured $\delta^{26}Mg$ values of biogenic $CaCO_3$. Mg isotope values are expressed as per mil (‰) deviation from the isotope composition of seawater reference material, BCR-403.

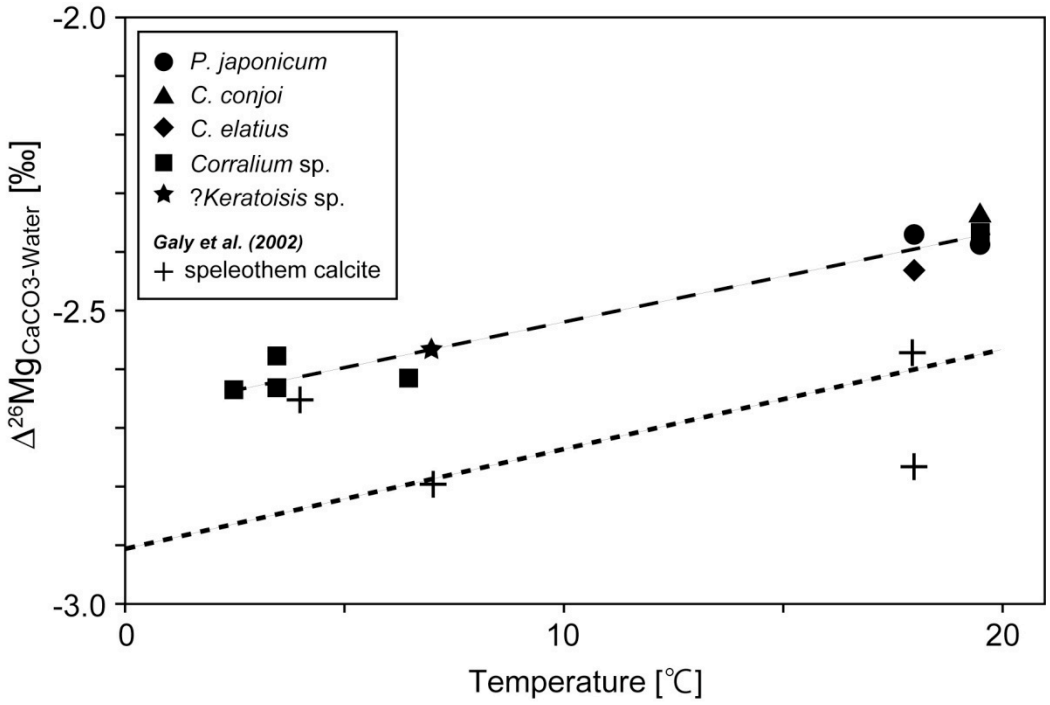

Fig. 9 Temperature dependence of Mg isotope fractionation of deep-sea corals. The dashed line denotes the regression equation: $1000*\ln(\alpha) = -2.68\ (\pm\ 0.04) + 0.0157\ (\pm\ 0.0030)*T$ (ºC). Dotted line represents that of inorganically precipitated calcite (Galy et al., 2002).

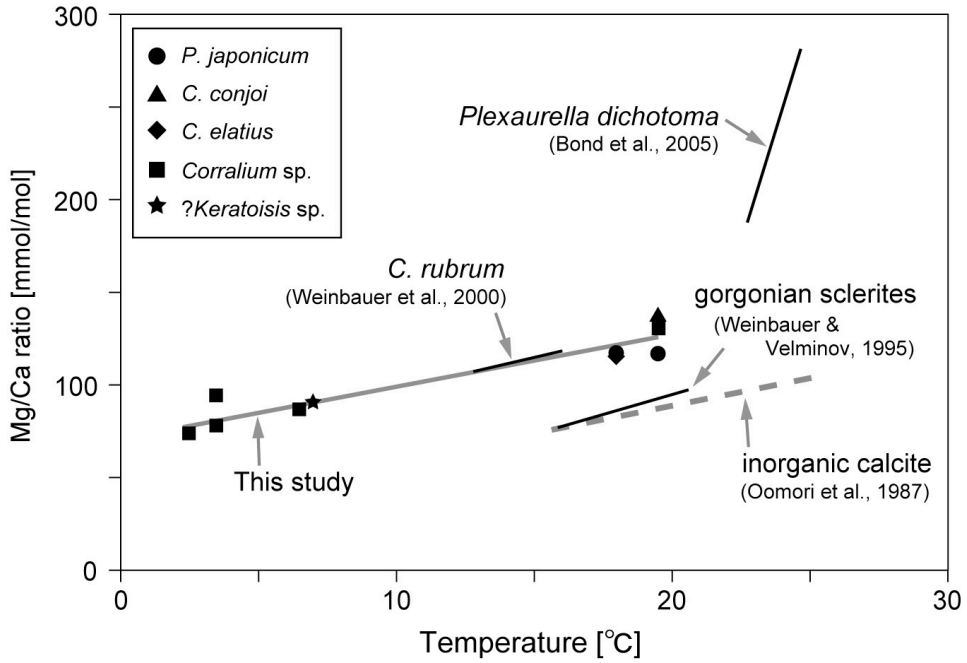

Fig. 10 Comparison of Mg/Ca-temperature in deep-sea corals and inorganic calcite. The obtained regression of this study was very similar to the previously reported equation of *C. rubrum* (Weinbauer et al., 2000).

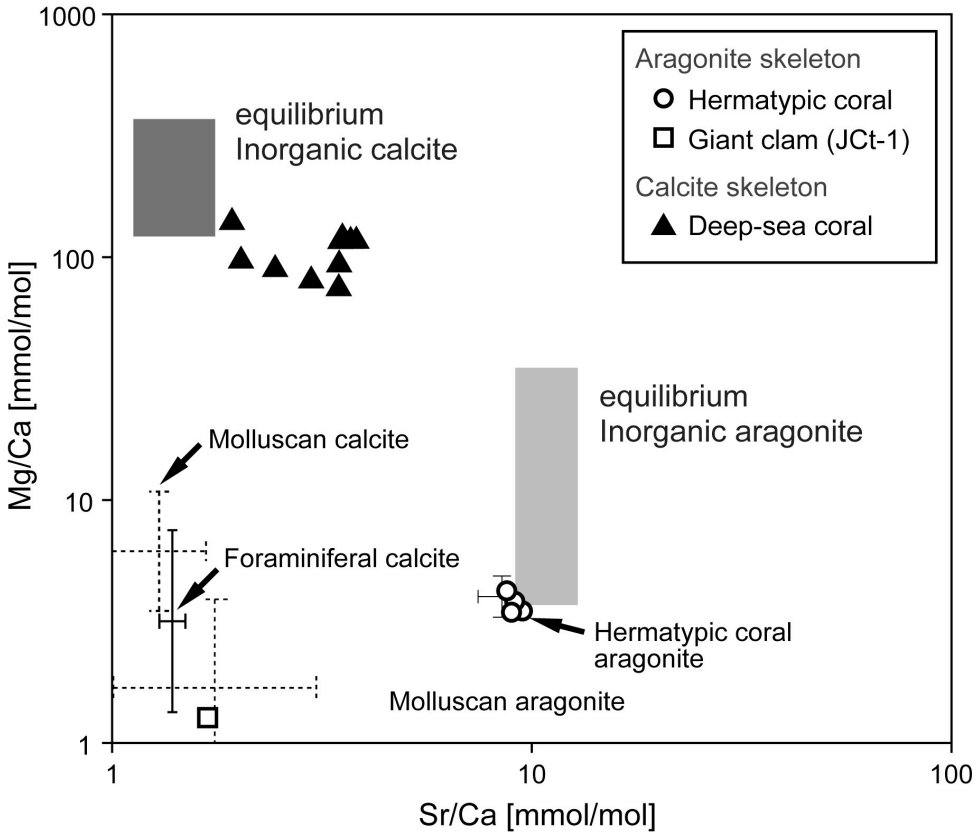

Fig. 11 The correlation between Mg/Ca and Sr/Ca ratios of the specimens of this study compared to biogenic and inorganic $CaCO_3$. The schematic plot is modified from Rosenheim et al. (2005). The circles, square and triangles represent the values of hermatypic corals, giant clam and deep-sea corals, respectively. The values of organisms are taken from Carpenter and Lohmann (1992) and Rosenheim et al. (2005). The boxes represents equilibrium values of inorganic calcite and aragonite taken from Reeder (1990).

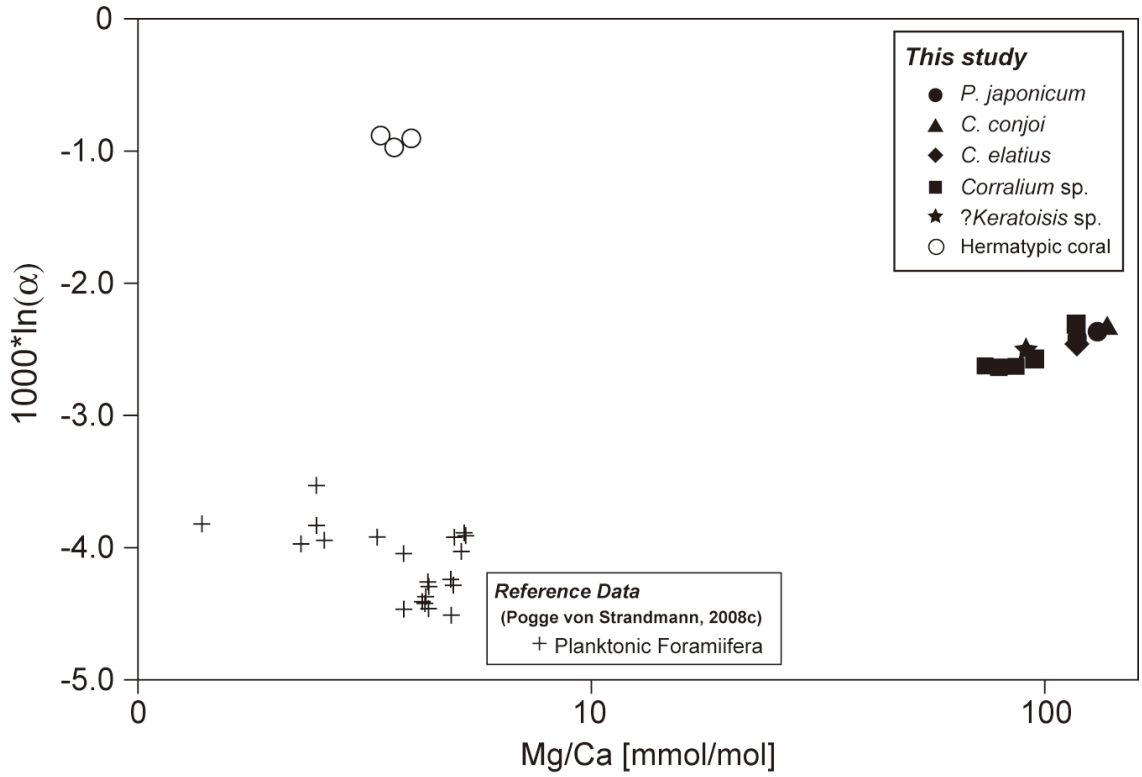

Fig. 12 The correlation between δ^{26}Mg values and Mg/Ca ratios of biogenic calcite and aragonite. The crosses represent the data of foraminifera from Pogge von Strandmann (2008c). Note that the original data of Pogge von Strandmann (2008c) have been converted to δ^{26}Mg relative to seawater.

Sample ID	Sample details			
	Name	Mineralogy	Location	Lat/Log
Seawater				
IRMM BCR403	Reference material	-	North Sea	
KH98-3 CM06	–	-	North Pacific	
KH03-1-st1	-	-	East Pacific	
KH04-5-st5	-	-	Antarctic Sea	
KH04-5-st6	-	-	Antarctic Sea	
Scleractian Coral				
OGA02-1-1	*Porites* sp.	Aragonite	Northwest Pacific	27°N 142°W
OGA02-1-2	*Porites* sp.	Aragonite	Northwest Pacific	27°N 142°W
KKI08-01	*Porites* sp. (fossil)	Aragonite	Northwest Pacific	28°N 129°W
SSK08-1-K	*Acropora* sp.	Aragonite	Northwest Pacific	26°N 127°W
SSK08-2-A	*Acropora* sp.	Aragonite	Northwest Pacific	26°N 127°W
Deep-sea Coral				
DPC-1-KCC	*C. konojoi*	Calcite	Northwest Pacific	32°N 134º′W
DPC-1-23-T1	*C. konojoi*	Calcite	Northwest Pacific	32°N 134º′W
DPC-K1	*P. japonicum*	Calcite	Northwest Pacific	32°N 134º′W
DPC-12	*P. japonicum*	Calcite	Northwest Pacific	25°N 126°W
DPC-0812-B	*C. Elutis*	Calcite	Northwest Pacific	25°N 126°W
DPC-0812-R	*C. Elutis*	Calcite	Northwest Pacific	25°N 126°W
DPC-0812-W	*C. Elutis*	Calcite	Northwest Pacific	25°N 126°W
DPC-14-3B-6	?*Keratoisis* sp.	Calcite	Northwest Pacific	27°N 142°W
DPC-K4	*Corallium* sp.	Calcite	Northwest Pacific	32°N 132°W
DPC-K3	*Corallium* sp.	Calcite	Northwest Pacific	27°N 142°W
DPC-727	*Corallium* sp.	Calcite	North Pacific	28°N 177°W
DPC-K2	*Corallium* sp.	Calcite	North Pacific	28°N 177°W
DPC-K5	*Corallium* sp.	Calcite	North Pacific	28°N 177°W
Carbonate Reference Material				
JCp-1	*Porites* sp.	Aragonite	Northwest Pacific	24°N 124º′W
JCt-1	*Tridacna gigas* (fossil)	Aragonite	Northwest Pacific	26°N 126º′W

Table 1 Sample locality and environmental information.

Sample ID	Location	Depth (m)	$d^{25}Mg$	2s	$d^{26}Mg$	2s
Seawater						
IRMM BCR403	North Sea	-	0.02	0.01	0.05	0.01
			0.02	0.07	0.01	0.13
			-0.01	0.08	0.00	0.19
			0.02	0.07	0.01	0.13
			-0.01	0.08	0.00	0.19
			-0.04	0.01	-0.02	0.02
KH98-3 CM06 5m	North Pacific	5	-0.04	0.06	-0.09	0.08
KH03-1-st1	East? Pacific	50	0.02	0.05	0.06	0.08
KH04-5-st5	Antarctic Sea	3500	0.01	0.03	-0.04	0.08
KH04-5-st6	Antarctic Sea	50	-0.01	0.05	0.01	0.05

Table 2 Results of Mg isotope ratios of seawater samples. The 2σ is gained from triplicate repeats of each sample.

Sample ID	T [ºC]	δ^{25}Mg	2σ	δ^{26}Mg	2σ	Mg/Ca	Sr/Ca	Ba/Ca	U/Ca
Carbonate Reference Material									
JCp-1		-0.58	0.05	-1.12	0.06	4.19	8.72	2.06	3.53
		-0.55	0.02	-1.05	0.04				
		-0.52	0.11	-1.00	0.13				
		-0.58	0.07	-1.11	0.08				
		-0.57	0.08	-1.07	0.12				
		-0.58	0.23	-1.08	0.53				
		-0.60	0.22	-1.14	0.54				
JCt-1		-1.34	0.03	-2.54	0.06	1.27	1.70	1.22	0.06
		-1.34	0.15	-2.61	0.33				
		-1.34	0.14	-2.60	0.26				
		-1.30	0.12	-2.57	0.19				
Scleractian Coral									
OGA02-1-1 (without tissue)		-0.49	0.06	-0.97	0.13	3.69	9.09	11.52	3.77
OGA02-1-2 (with tissue)		-0.50	0.24	-0.95	0.34	-	-	-	-
KKI08-01		-0.45	0.05	-0.87	0.08	3.43	8.98	1.13	3.76
SSK08-1-K		-0.45	0.03	-0.89	0.04	3.45	9.47	1.10	4.45
SSK08-2-A		-0.48	0.06	-0.90	0.18	4.04	9.51	1.31	4.27
Deep-sea Coral									
DPC-1-23-T1	19.5	-1.24	0.08	-2.39	0.15	116.56	3.78	0.99	0.56
	19.5	-1.23	0.03	-2.41	0.02				
DPC-1-KCC	19.5	-1.20	0.13	-2.34	0.22				
DPC-12	18	-1.18	0.02	-2.30	0.05	116.71	3.50	2.54	0.36
	18	-1.27	0.08	-2.44	0.11				
DPC-K1	19.5	-1.20	0.07	-2.33	0.14	137.40	1.93	1.16	0.59
DPC-0812-B	18	-1.25	0.00	-2.45	0.07	116.65	3.70	0.63	0.27
DPC-0812-R	18	-1.24	0.04	-2.43	0.05	121.43	3.53	0.59	0.35
DPC-0812-W	18	-1.23	0.04	-2.41	0.07	121.60	3.54	0.58	0.35
DPC-14	7	-1.27	0.03	-2.51	0.05	90.93	3.46	2.67	0.20
	7	-1.32	0.10	-2.62	0.26				
DPC-K4	19.5	-1.21	0.08	-2.36	0.17	130.94	0.17	1.98	0.51
DPC-727	2.5	-1.32	0.05	-2.61	0.08	73.75	3.45	4.25	0.41
	2.5	-1.35	0.07	-2.65	0.07				
DPC-K2	3.5	-1.35	0.09	-2.57	0.27	94.54	2.03	2.48	0.42
DPC-K3	6.5	-1.33	0.13	-2.61	0.19	86.59	2.46	2.29	0.32
DPC-K5	3.5	-1.35	0.05	-2.63	0.07	78.40	2.98	2.72	0.12

Table 3 Results of Mg isotope ratios and the concentrations of minor and trace elements. The 2σ is gained from triplicate repeats of each sample.